The Astrophysical Journal, 617:1330–1346, 2004 December 20

INITIAL RESULTS FROM THE PALOMAR ADAPTIVE OPTICS SURVEY OF YOUNG SOLAR-TYPE STARS: A BROWN DWARF AND THREE STELLAR COMPANIONS

Stanimir A. Metchev and Lynne A. Hillenbrand
Division of Physics, Mathematics, and Astronomy, California Institute of Technology, MS 105-24, Pasadena, CA 91125;
metchev@astro.caltech.edu, lah@astro.caltech.edu
Received 2004 May 20; accepted 2004 August 27

ABSTRACT

We present first results from the Palomar Adaptive Optics Survey of Young Stars conducted at the Hale 5 m telescope. Through direct imaging we have discovered a brown dwarf and two low-mass stellar companions to the young solar-type stars HD 49197, HD 129333 (EK Dra), and V522 Per and confirmed a previously suspected companion to RX J0329.1+0118 (Sterzik et al.), at respective separations of 0.″95 (43 AU), 0.″74 (25 AU), 2.″09 (400 AU), and 3.″78 (380 AU). Physical association of each binary system is established through common proper motion and/or low-resolution infrared spectroscopy. Based on the companion spectral types, we estimate their masses at 0.06, 0.20, 0.13, and 0.20 $M_{\odot}$, respectively. From analysis of our imaging data combined with archival radial velocity data, we find that the spatially resolved companion to HD 129333 is potentially identical to the previously identified spectroscopic companion to this star (Duquennoy & Mayor). However, a discrepancy with the absolute magnitude suggests that the two companions could also be distinct, with the resolved one being the outermost component of a triple system. The brown dwarf HD 49197B is a new member of a growing list of directly imaged substellar companions at 10–1000 AU separations from main-sequence stars, indicating that such brown dwarfs may be more common than initially speculated.

Subject headings: binaries: close — instrumentation: adaptive optics — stars: individual (HD 49197, HD 129333, V522 Persei, RX J0329.1+0118) — stars: low-mass, brown dwarfs

1. INTRODUCTION

High-contrast imaging searches for low-mass companions to nearby and/or young stars have increased dramatically in number since the initial discovery of a brown dwarf companion to a main-sequence star (Gl 229) through direct imaging (Nakajima et al. 1995). One particularly powerful technique is adaptive optics (AO), which provides the high angular resolution ($\lesssim$0.″1) achievable at the diffraction limit of large ground-based telescopes. The widening niche of high-contrast imaging opened by recent developments in AO technology implies that not only brown dwarfs but also exosolar planets may be within the realm of direct imaging. Nowadays nearly every ground-based telescope equipped with an AO system hosts an imaging companion search project. The sudden explosion in interest in this topic has been fueled by the success of the radial velocity (r.v.) method in detecting solar system analogs (e.g., Marcy & Butler 1998). Through longer time lines of observation and higher precision, the sensitivity of r.v. surveys has now extended outward to include planets at semimajor axes $\gtrsim$3 AU (Carter et al. 2003; Naef et al. 2004), i.e., near the Jovian region in the solar system. While the sensitivity of direct imaging to "planetary-mass" (1–13 Jupiter masses [M_J]; Burrows et al. 1997) objects at such separations from Sun-like stars is still extremely limited as a result of contrast requirements, several higher mass brown dwarf companions have been discovered at wider separations (see compilation in Reid et al. 2001), some at projected distances as small as 14–19 AU (Els et al. 2001; Liu et al. 2002). High-resolution spectroscopic monitoring and direct imaging are thus complementary in searching for substellar companions to stars. Future development of both methods promises to narrow and eventually close the sensitivity gap between them.

Young stars are the most suitable targets for direct imaging of substellar companions. At ages of 10–100 Myr the expected brightness ratio in the near-IR between a $10M_{\rm Jup}$ object and a solar-type star is 10^{-3} to 10^{-5} (Burrows et al. 1997; Baraffe et al. 2003). Modern AO systems can routinely achieve comparable dynamic range at 1″ separations from bright stars. Hence, for young stars within 40 pc of the Sun we can probe for massive planets at separations comparable to the giant planet region in our own solar system. However, few young stars are known at such small heliocentric distances. These are constrained to several tens of members of young moving groups, TW Hya (Rucinski & Krautter 1983; de La Reza et al. 1989), Tucana/Horologium (Zuckerman & Webb 2000; Zuckerman et al. 2001a), and β Pic (Zuckerman et al. 2001b), and have already been targeted with sensitive space-based and ground-based AO surveys, which have uncovered three to four brown dwarf companions (Lowrance 2001; Lowrance et al. 2003; Neuhäuser & Guenther 2004) but no planetary-mass ones.

Because contrast and projected separation are the limiting factors in detectability of substellar companions, brown dwarfs, being more luminous than planets, are detectable at greater heliocentric distances and at smaller angular separations from their host stars. At the same physical separation from the primary (e.g., 50–100 AU), brown dwarf companions should be detectable around older (several gigayears) and/or more distant ($\lesssim$200 pc) stars compared to planets, allowing a larger sample of targets. With regard to this, we have commenced a survey of young (<400 Myr) solar-type (F5–K5) stars within 160 pc using the AO system on the Palomar 5 m telescope. Our survey sample is largely a subset of the sample targeted by the Formation and Evolution of Planetary Systems (FEPS) *Spitzer* Legacy Team (Meyer et al. 2004). Although faint primary stars, such as M dwarfs or white dwarfs, offer more favorable contrast

TABLE 1
OBSERVATIONS

Target	First Epoch/Telescope	Mode	Second Epoch/Telescope	Mode
HD 49197	2002 Feb 28/Palomar	JHK_S coronagraphic imaging	2003 Nov 9–10/Keck II	JHK_S coronagraphic imaging, K spectroscopy
HD 129333	2003 Jan 12/Palomar	JHK_S noncoronagraphic imaging, JK spectroscopy	2003 May 13/Palomar	Brγ noncoronagraphic imaging
V522 Per	2003 Sep 20/Palomar	JHK_S noncoronagraphic imaging	2003 Nov 10/Keck II	K_SL' noncoronagraphic imaging, JK spectroscopy
RX J0329.1+0118	2003 Sep 21/Palomar	JHK_S coronagraphic imaging	2003 Nov 10/Keck II	K spectroscopy

for imaging substellar companions, we have chosen to limit our sample to solar analogs because of interest in determining the multiplicity statistics of substellar objects around other suns. Furthermore, several recent large surveys have already explored the multiplicity of nearby ($\lesssim$50 pc) cool stars (Close et al. 2003; Carson et al. 2003; McCarthy & Zuckerman 2004) or white dwarfs (Zuckerman & Becklin 1992; Green et al. 2000), while a large sample of F–G stars has not been studied because of comparatively small numbers in the immediate solar neighborhood.

Preliminary results from our survey were reported in Metchev et al. (2002). Here we present the strategy of the survey and the discovery and confirmation of resolved low-mass companions to HD 49197, HD 129333 (EK Dra), V522 Per, and RX J0329.1+0118. We refer to these throughout the paper as HD 49197B, HD 129333B, V522 PerB, and RX J0329.1+0118B. For convenience of notation, a second candidate companion to HD 49197 found to be an unrelated background star will be denoted as HD 49197"C". The full sample and further results from the survey will be discussed in a later paper.

2. OBSERVING STRATEGY

The observations described in this section are representative of our general survey observing strategy. Table 1 details the imaging and spectroscopic observations specifically for the four objects presented here. The properties of the observed primaries are given in Table 2.

2.1. *Imaging*

2.1.1. *First-Epoch Imaging and Survey Sample Subdivision*

First-epoch observations are obtained with the Palomar AO system (PALAO; Troy et al. 2000) in residence at the Cassegrain focus of the Palomar 5 m telescope. Since the summer of 2003 the wave front sensor runs at frame rates up to 2 kHz, and the system routinely produces diffraction-limited images (0.″09 at K_S) with Strehl ratios in the 30%–50% range at 2 μm on $V < 12$ mag guide stars and up to 75% on $V < 7$ mag guide stars. PALAO employs the Palomar High Angular Resolution Observer (PHARO; Hayward et al. 2001), a 1024×1024 pixel HgCdTe HAWAII detector with imaging (25 and 40 mas pixel^{-1} plate scale) and spectroscopic ($R = 500$–2000) capabilities in the near-IR. A set of coronagraphic spots, Lyot masks, and neutral density (ND) filters are available to achieve the desired dynamic range.

Our program entails K_S-band (2.15 μm) imaging in the 25 mas pixel^{-1} mode ($25'' \times 25''$ field of view [FOV]) both with and without a 0.″97 diameter coronagraphic stop. For high dynamic range, long (1 minute) coronagraphic images are taken to identify fainter (potentially substellar) companions at separations greater than 0.″5. Twenty-four such exposures are taken, for a total of 24 minute integration per target, with 6 minutes spent at each of four different orthogonal detector orientations (obtained by rotating the Cassegrain ring of the telescope). For every 6 minutes of on-target imaging (i.e., at each detector orientation), separate 1 minute coronagraphic exposures are taken at five dithered sky positions $32''$–$60''$ from the star. For high angular resolution (but with lower dynamic range), short (1.4–9.8 s) noncoronagraphic exposures are taken to look for close companions of modest flux ratio and to establish relative photometric calibration. The images are taken in a five-point dither pattern at the vertices and center of a box $6''$ on a side. A 1% transmission ND filter is used if necessary to avoid saturation.[1]

[1] The ND 1% filter was calibrated photometrically through repeated (17–20 per band) observations of three program stars with and without the filter, and its extinction was measured at 4.753 ± 0.039 mag at J, 4.424 ± 0.033 mag at H, and 4.197 ± 0.024 mag at K_S.

TABLE 2
PROPERTIES OF THE OBSERVED STARS

Object	Proper Motion (mas yr^{-1}) $\mu_\alpha \cos\delta$	Proper Motion (mas yr^{-1}) μ_δ	Parallax (mas)	Spectral Type	K_S[a] (mag)	Age[b] (Myr)	Notes
HD 49197	-35.12 ± 1.05	-48.59 ± 0.63	22.41 ± 0.87	F5 V	6.067 ± 0.024	260–790	1, 3
HD 129333	-138.61 ± 0.61	-11.92 ± 0.68	29.46 ± 0.61	G0 V	5.914 ± 0.021	10–100	1, 4
V522 Per	17.6 ± 3.0	-26.9 ± 2.7	5.46 ± 0.20	...	9.352 ± 0.024	90 ± 10	2, 5
RX J0329.1+0118	5.4 ± 1.1	-5.8 ± 1.1	$\lesssim$10	G0 IV	9.916 ± 0.019	$\approx$120	2, 6, 7

NOTES.—(1) Proper motion and parallax from *Hipparcos* (Perryman et al. 1997). (2) Proper motion from Tycho 2 (Høg et al. 2000). (3) Spectral type from *Hipparcos* (Perryman et al. 1997). (4) Spectral type from Buscombe & Foster (1997). (5) Assumed to be at the mean *Hipparcos* distance (van Leeuwen 1999) of the α Per cluster. (6) A distance of at least 100 pc can be inferred for this young ($\sim$100 Myr; Frink et al. 1997) star from its small proper motion and its location toward the Taurus star-forming region. (7) Spectral type from Buscombe (1998).

[a] From the 2MASS Point Source Catalog (Cutri et al. 2003).

[b] See § 4.2.

On occasion, a narrowband (1%) Brγ (2.17 μm) filter is used for higher throughput, instead of the ND 1% filter.

To avoid detector saturation and/or decreased sensitivity over a substantial fraction of the image area, stars with bright ($\Delta K_S < 4$) projected companions in the PHARO field of view were not observed with deep coronagraphic exposures. However, binaries with separation $\leq$0.″5 were included, as both components of the binary could then be occulted by the coronagraph. This naturally splits our survey sample into two groups: the "deep" subsample, consisting of essentially single stars and close binaries, and the "shallow" subsample, encompassing the remaining stars. Membership to one of the two subsamples was assigned at the telescope, when their multiplicity and approximate flux ratio were revealed during the short exposures. The shallow subsample was further expanded to include stars out to 200 pc and/or older than 400 Myr to cover the entire FEPS sample accessible from the Northern hemisphere.

Short dithered exposures were taken of all stars, while long coronagraphic exposures were taken only of stars in the deep subsample at K_S band. In addition, short J- (1.22 μm) and H-band (1.65 μm) exposures were taken of all candidate binaries (all stars in the shallow survey and the less than 0.″5 systems in the deep survey) to allow approximate photospheric characterization of the components.

In accordance with the above distinction, HD 49197 was observed for a total of 24 minutes with the coronagraph as a part of the deep survey, while HD 129333, RX J0329.1+0118 (with bright candidate companions), and V522 Per (α Per member, 190 pc from the Sun; van Leeuwen 1999) were observed only with short exposures. Conditions were photometric during the first-epoch observations of HD 49197, V522 Per, and RX J0329.1+0118 and unstable during those of HD 129333.

2.1.2. *Follow-up Imaging*

We obtain second-epoch imaging observations of all candidate companions to check for common proper motion with their corresponding stars. Such were taken for HD 129333 with PALAO/PHARO and for HD 49197, V522 Per, and RX J0329.1+0118 with NIRC2 (K. Matthews et al. 2004, in preparation) and the Keck II AO system (diffraction limit 0.″05 at K_S; Wizinowich et al. 2000). Conditions were not photometric during follow-up, and only the best images (Strehl ratio $S \gtrsim 40\%$) were selected for astrometry. HD 129333 was followed up in the narrowband Brγ filter, which allowed higher throughput than the ND 1% filter in the shortest (1.4 s) PHARO exposures. Given the unstable atmospheric conditions during the second-epoch imaging of HD 129333, this allowed us to take high signal-to-noise ratio (S/N) exposures on timescales that would most finely sample the variations in the seeing and to select only the ones with the best imaging quality.

Keck follow-up is done at JHK_S, or at K_SL' if the candidate companion is expected to be bright enough to be seen at L' (given $0.7 < K_S - L' < 2.5$ for L and T dwarfs; Leggett et al. 2002). Sequences of short (up to 20 s from multiple co-adds) dithered noncoronagraphic and long (1 minute) target-sky-target exposures are taken with a 1″ or 2″ diameter coronagraph in the same manner as with PHARO, although without detector rotations. The candidate companions are exposed until an S/N comparable to that in the first-epoch PHARO observation is achieved (for similar positional accuracy), up to 6 minutes per filter in J, H, and K_S. The total integration time at L' is up to 10.5 minutes, which allows the detection of $L' \lesssim 15.0$ objects. We mainly use the 40 mas pixel^{-1} (wide) NIRC2 camera (41″ FOV), which severely undersamples the Keck AO point-spread function (PSF) but is known to suffer from less distortion than the 20 mas pixel^{-1} (medium) camera over the same field (Thompson et al. 2001). Although we also have the option of using the 10 mas pixel^{-1} (narrow) camera (10″ FOV) in NIRC2, it does not allow follow-up of distant candidate companions, and we avoid using it for consistency with the other NIRC2 observations.

2.1.3. *Imaging Data Reduction*

All imaging data are reduced in a standard fashion for near-IR observations. Flat fields are constructed from either images of the twilight sky (for the Palomar data) or images of the lamp-illuminated dome interior (for the Keck data). A bad pixel mask is created from the individual flats, based on the response of each pixel to varying flux levels. Pixels whose gain deviates by more than 5 σ from the mode gain of the array are flagged as bad. Sky frames for the dithered, noncoronagraphic exposures are obtained by median-combining four of the five exposures in the dither pattern (excluding the central pointing) and rejecting the highest pixel value in the stack. The coronagraphic-mode sky frames are median-combined using an average sigma clipping algorithm to remove pixels deviant by more than 5 σ. The sky-subtracted images of each target are divided by the flat field and then registered and median-combined to create a final high-S/N image (Figs. 1 and 2). However, photometric and astrometric measurements are performed on the individual reduced images.

No PSF stars are observed at either Palomar or Keck. With PHARO at Palomar, median-combined images from all four detector orientations can be used to reproduce an approximate PSF. This approach was chosen to emulate the observation of separate PSF stars of identical brightness and color, while optimizing the time spent on science targets. However, we have found that a simple 180° rotation and subtraction technique works equally well, and we use that on both the Palomar and Keck data. While neither approach eliminates telescopic speckle noise (as could be the case if actual PSF stars were observed), both significantly reduce point-symmetric structure in the PSF.

2.2. *Astrometric Calibration*

The exact pixel scale of the 25 mas PHARO camera was determined using known binary stars from the Sixth Orbit Catalog (Hartkopf et al. 2001; Hartkopf & Mason 2003a): WDS 09006+4147 (grade 1; Hartkopf et al. 1996), WDS 16147+3352 (grade 4; Scardia 1979), WDS 18055+0230 (grade 1; Pourbaix 2000), and WDS 20467+1607 (grade 4; Hale 1994). These "calibration binaries" are observed throughout our campaign at Palomar at all four detector orientations. The combination of grade 1 (accurately determined, short period) orbits and grade 4 (less accurately known, longer period) orbits was selected from the list of astrometric calibrators recommended by Hartkopf & Mason (2003b). Despite the lower quality of the solution for binaries with grade 4 orbits, their periods are generally much longer (889 and 3249 yr for WDS 16147+3352 and WDS 20467+1607, vs. 21.78 and 88.38 yr for WDS 09006+4147 and WDS 18055+0230, respectively), so their motions are predicted with sufficient accuracy for many years into the future. The mean pixel scale of PHARO was measured to be 25.22 mas pixel^{-1} with a 1 σ scatter of 0.11 mas pixel^{-1} among measurements of the individual binaries at different detector orientations. This measurement is consistent with, although less precise than, our previous determination (25.168 ± 0.034 mas pixel^{-1}; Metchev et al. 2003), which was obtained from only one calibration binary at a single Cassegrain ring orientation. The larger scatter of

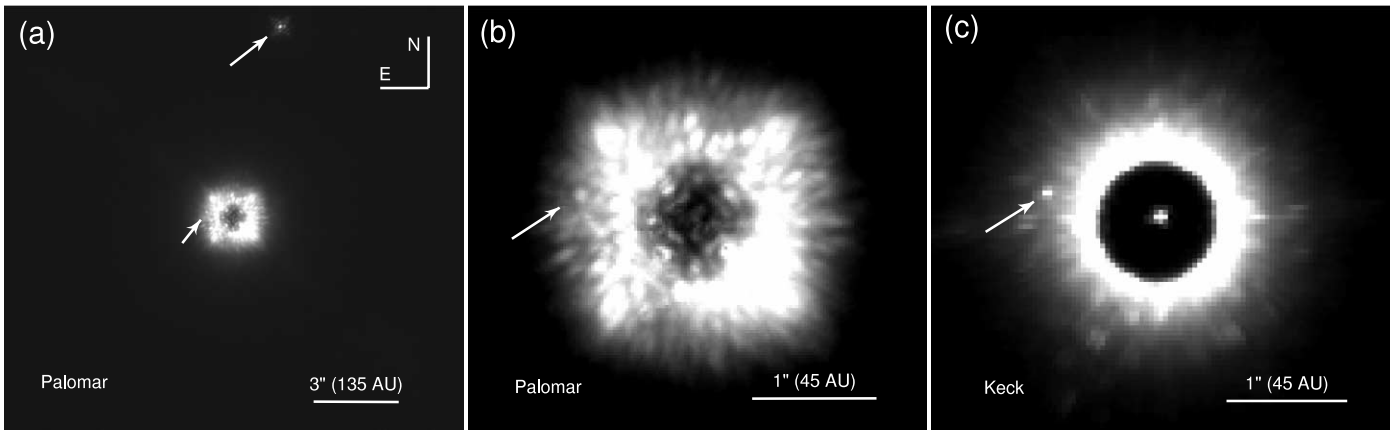

FIG. 1.—K_S-band (2.15 μm) (*a*, *b*) first- and (*c*) second-epoch images of HD 49197. Panel (*a*) shows both candidate companions to HD 49197; panels (*b*) and (*c*) are zoomed in to point out only the close-in bona fide companion (HD 49197B). The first-epoch image is the result of 24 median-combined 60 s exposures with Palomar/PHARO, whereas the second-epoch image was formed by median-combining six 60 s exposures with Keck/NIRC2. A 1.″0 diameter coronagraph occults the primary in both cases; in the Keck image the coronagraph shows a residual ≈0.16% transmission. HD 49197B was initially unnoticed in the first-epoch image, where its detection was hindered by the presence of equally prominent AO speckles.

our more recent measurement is indicative of the systematics involved in choosing different calibration binaries and in observing at more than one detector orientation.

The plate scale of the wide NIRC2 camera was calibrated using the binary WDS 15360+3948 (grade 1; Söderhjelm 1999). The obtained value of 39.82 ± 0.25 mas pixel^{-1} is consistent with the preship measurement of 39.7 ± 0.5 max pixel^{-1}.[2] Because only one binary was used for calibrating NIRC2, a 0.63% error term corresponding to the uncertainty in the semimajor axis of the binary has been added in quadrature to the uncertainty of our measurement.

2.3. *Spectroscopy*

2.3.1. *Observations*

Spectroscopy of faint targets in the halos of bright objects is more challenging than spectroscopy of isolated targets. Care needs to be taken to achieve optimum suppression of the scattered light of the bright stars by either using a coronagraph (in a manner similar to coronagraphic imaging) or aligning the slit so as to minimize light admitted from the halo. Since neither PHARO nor NIRC2 allows coronagraphic spectroscopy, when taking spectra of faint companions we orient the slit as close as possible to 90° from the primary-companion axis. Spectra of brighter companions, for which the signal from the halo is negligible compared to that from the target, are obtained by aligning the binary along the slit. Given that we often use the F5–K5 IV–V primaries in our sample as telluric standards, such alignment improves our observing efficiency. Sky spectra are obtained simultaneously with the target spectra, by dithering the targets along the slit.

Promising candidate companions are observed at medium resolution ($R = 1000$–3000) at K and (AO correction permitting) J. In PHARO we use the corresponding grism and filter combination (K or J) and the 40 mas pixel^{-1} camera, while in NIRC2 we use the K or J filter with the "medres" grism and the wide (40 mas pixel^{-1}) camera. For K-band spectroscopy in first order with PHARO and in fifth order with NIRC2 we achieve complete coverage of the 2.2 μm atmospheric window. For J-band spectroscopy in first order with PHARO the coverage is limited by the size of the detector to a 0.16 μm bandwidth. J-band spectroscopy with NIRC2 can cover the entire 1.2 μm window, but the spectrum is split between the fifth and the sixth dispersion orders. To allow simultaneous data acquisition from both orders, we fit both onto the wide camera by clipping the fifth (longer wavelength) order shortward of 1.22 μm

[2] See http://www2.keck.hawaii.edu/inst/nirc2/genspecs.html.

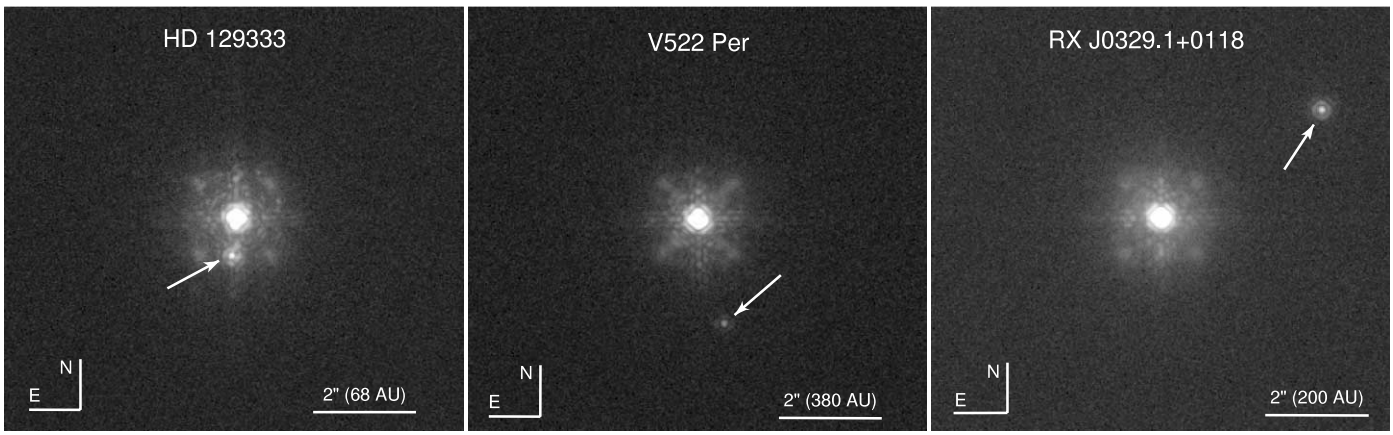

FIG. 2.—Palomar images of the stellar companions. The HD 129333 image is taken through a narrowband (1%) Brγ (2.166 μm) filter, while the V522 Per and RX J0329.1+0118 images are taken at K_S. Five dithered 1.4 s exposures were aligned and median-combined to obtain each of the displayed images.

and the sixth (shorter wavelength) order longward of 1.28 μm. The combined *J*-band spectrum has complete coverage between 1.16 and 1.35 μm.

We took *J*- and *K*-band spectra with PHARO of HD 129333A/B, *J* and *K* spectra with NIRC2 of V522 PerA/B, and *K*-band NIRC2 spectra of HD 49197A/B and RX J0329.1+0118A/B. For the observations of HD 129333 with PHARO and of RX J0329.1+0118 with NIRC2, the binary was aligned along the slit, whereas spectra of the other two binaries (with fainter companions) were obtained by placing each component in the slit individually. A 0.″26 (6.5 pixel) slit was used in PHARO, and a 0.″08 (2 pixel) slit was used in NIRC2, resulting in spectral resolutions of 1200 at *J* and 1000 at *K* with PHARO and 2400 at fifth-order *J* (1.22–1.35 μm), 2900 at sixth-order *J* (1.15–1.28 μm), and 2700 at *K* with NIRC2.

Flat fields with the dispersive grisms in place were not obtained for any of our spectroscopic observations. Instead, the raw spectra were divided by an imaging flat field, constructed in the same manner as for the imaging observations. The flat-fielded spectra were corrected for bad pixels, using the same bad pixel mask as in the imaging case. Strong positive deviations due to cosmic-ray hits were then eliminated using the L.A. Cosmic Laplacian filter algorithm (van Dokkum 2001). Fringing was at a noticeable level (≈15%) only in spectra obtained with PHARO (of HD 129333) and was reduced to below 5% by dividing the target spectrum by that of the telluric standard, taken at a nearby position on the detector.

2.3.2. *Spectroscopic Data Reduction*

Extraction of the spectra is performed using IRAF *apextract* tasks. To reduce contamination from the halo of the primary in the companion spectra, the local background (arising mostly from the halo) is fitted by a first-order polynomial along the direction perpendicular to the dispersion axis and subtracted during extraction. In addition, the aperture width for the companion spectrum is conservatively set to the FWHM of the profile so as to include only pixels with maximum S/N. Pixels within the aperture are summed along detector columns (which are nearly perpendicular to the dispersion axis), and the resulting "compressed" spectrum is traced along the dispersion axis by fitting a high-order (8–15) Legendre polynomial. The tracing step is approximately equal to the slit width, where at each step the data point is obtained as the sum of 3–10 adjacent pixels (1.5–3 slit widths, the spectra of fainter objects being more heavily averaged) in the compressed spectrum. This procedure is found to produce consistent results for extractions of multiple dithered spectra of the same companion, indicating that scattered light contamination from the primary has been reduced to a small level. Nevertheless, in some cases of very faint close-in companions, the continuum shape is still found to vary noticeably among the individual extractions. We therefore avoid classifying the spectra of the companions based on their continuum shapes but rely on the relative strengths of narrow absorption features (discernible given our resolution) instead (§ 3.3).

A dispersion solution for each spectrum is obtained from night sky lines in non–sky-subtracted images, using the task *identify* and OH emission line lists available in IRAF. For the spectra of primaries observed separately (e.g., HD 49197 and V522 Per), whose shallower (10–120 s) exposures do not contain telluric emission lines at a high enough S/N to allow the fitting of a dispersion solution, such is derived after registration with deeper (10–15 minute long) companion spectra taken immediately after those of the primaries. The tasks *fxcor* and *specshift* are used to cross-correlate and align the individual wavelength-calibrated spectra for a given object. The individual primary and companion spectra are then median-combined using *scombine*.

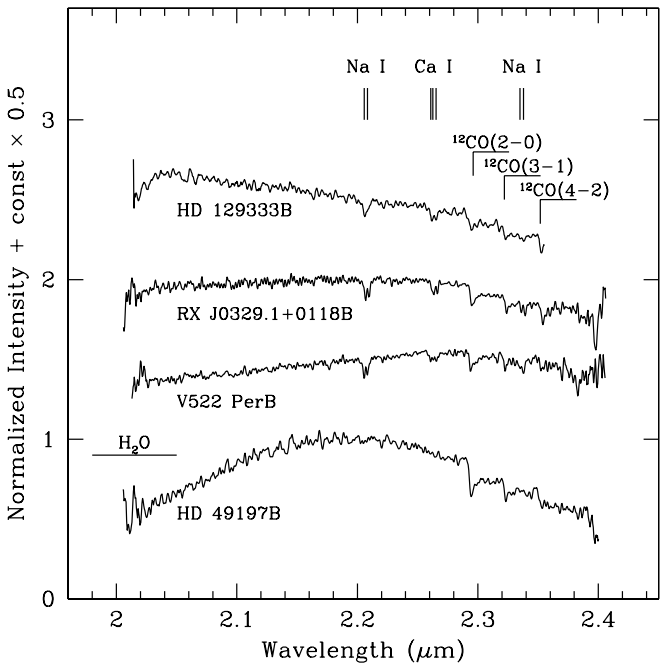

FIG. 3.—*K*-band spectra of the low-mass companions from Palomar (HD 129333B; $R \approx 1000$) and Keck (RX J0329.1+0118B, V522 PerB, and HD 49197B; $R \approx 2700$). All spectra have been normalized to unity at 2.20 μm and offset by 0.5 in the vertical axis.

Since the primaries (when earlier than K0) double as telluric standards, their spectra are first corrected for photospheric absorption from atomic hydrogen (H Pβ at 1.282 μm and H Brγ at 2.166 μm) by hand-interpolating over the absorption with the task *splot*. Weaker absorption features due to Na I, Ca I, Si I, Al I, and Fe I, although present in the spectra of our telluric standards, are left uncorrected because of blending (at our resolution) with various OH absorption lines in the Earth's atmosphere. After thus correcting the telluric spectra, the spectra of the companions are divided by those of the telluric standards. Finally, the spectra of the companions are multiplied by blackbodies with temperatures corresponding to the spectral types of the telluric standards (based on effective temperature vs. spectral type data from Cox 2000) and boxcar-smoothed by the width of the slit.

The above reduction procedure applies in exact form for NIRC2 spectra, which do not suffer from fringing. For PHARO data, which are noticeably affected by fringing, we divide the individual target spectra by those of the telluric standard before median-combining and wavelength calibration, since fringing depends on detector position, not on the dispersive element.

Reduced spectra for the objects reported here are presented in Figures 3 and 4. The mismatch in the continuum slopes between the fifth- and sixth-order *J*-band spectra of the companion to V522 Per may be due to our use of imaging, instead of spectroscopic flats.

3. ANALYSIS

3.1. *Photometry*

Broadband near-IR photometry of the companions is presented in Table 3. The measured quantity in each case is the

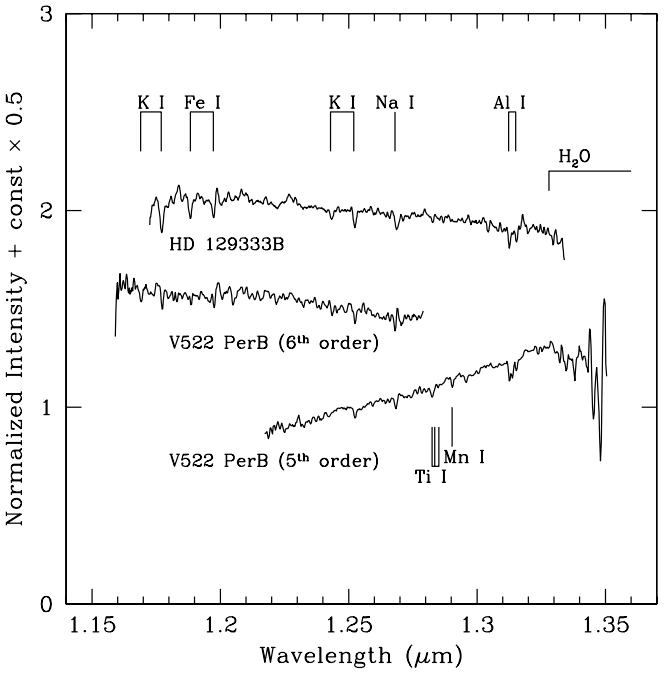

FIG. 4.—*J*-band spectra of two of the low-mass companions from Palomar (HD 129333B; $R \approx 1200$) and Keck (V522 PerB; $R \approx 2400$ in the fifth order and $R \approx 2900$ in the sixth). All spectra have been normalized to unity at 1.25 μm and offset by 0.5 in the vertical axis.

relative flux (ΔJ, ΔH, ΔK_S, $\Delta L'$) of the companion with respect to that of the primary. When the companions were visible without the coronagraph (in all cases except for the close-in companion to HD 49197), the fluxes of both components were measured directly from the short-exposure noncoronagraphic images. Flux ratios for the HD 129333, V522 Per, RX J0329.1+0118, and HD 49197A/"C" systems were obtained from the Palomar images in apertures of radii of 0.″2 ($2\lambda/D$ at K_S). For the photometry of HD 129333B we subtracted the halo of the nearby (0.″74) primary (as detailed in § 2.1.3) to minimize its contribution to the flux of the secondary. In the case of the HD 49197A/B system, the 0.″95 companion is not seen in PHARO images taken without the coronagraph, and only coronagraphic exposures were obtained with NIRC2. The magnitude of the companion was obtained with respect to the residual flux of the primary seen through the 1″ NIRC2 coronagraphic spot. The flux measurements were performed on the PSF-subtracted NIRC2 images in a 0.″16 radius ($3.2\lambda/D$ at K_S) aperture. The transmission of the spot was established from photometry of another program star in images taken with and without the 2″ coronagraph: its extinction was measured at 9.27 ± 0.07 mag at J, 7.84 ± 0.03 mag at H, and 7.19 ± 0.03 mag at K_S. The companion was seen in all six 1 minute coronagraphic exposures at K_S, but because of varying photometric conditions and proximity of diffraction spikes, it was detected in only three out of six PSF-subtracted exposures at H, and one out of six at J.

Sky values for each of the observed objects were determined as the centroid of the flux distribution in a 0.″1 wide annulus with an inner radius larger by λ/D than the distance at which the radial profile of the object fell below the level of the local background. For the primaries observed with PHARO this inner radius was 2.″0 ($20\lambda/D$ at K_S), while for HD 49197A, the flux of which was measured through the NIRC2 coronagraph, the inner radius was 0.″2 ($5\lambda/D$). For the companions, the inner radius of the sky annulus varied from 2.25 to 4 times the K_S diffraction limit, depending on whether the local background was strongly influenced by the halo of the primary (as near HD 49197 and HD 129333) or not. Experiments with varying sky annulus sizes in the two more detached systems (V522 Per and RX J0329.1+0118) showed that the relative photometry between two objects in the same image is preserved to within 0.08 mag for annuli ranging between 2.25 and $20\lambda/D$ in inner radius.

The $J - H$ and $H - K_S$ colors and K_S magnitudes are derived from the measured relative photometry by adopting the Two Micron All Sky Survey (2MASS; Cutri et al. 2003) magnitudes for the primaries. The $K_S - L'$ color of the companion to V522 Per was calculated assuming $K_S - L' = 0.04$ for the F5 V primary (Bessell & Brett 1988). A near-IR color-color diagram of the detected companions is presented in Figure 5. Extinction corrections of $A_J = 0.087$, $A_H = 0.055$, $A_K = 0.033$, and $A_L = 0.016$ have been applied to the colors of V522 PerB, based on $E(B - V) = 0.10$ toward the α Per cluster as measured by Pinsonneault et al. (1998). We have adopted $A_V = 3.1E(B - V)$ and the interstellar extinction law of Cardelli et al. (1989).

Based on the colors and the ΔK_S magnitudes, we can infer that HD 49197"C" is a likely F–G background star, whereas the remaining companions are consistent with being late-type stars associated with their primaries.

3.2. *Astrometry*

Three of the four systems were observed at two different astrometric epochs. RX J0329.1+0118 was observed only once, although prior-epoch astrometric data for it exist from Sterzik et al. (1997). Table 4 details for each binary the observed offset and position angle of the companion from the primary during the first and second epochs of observation, as well as the estimated offset and position angle during the first epoch, had the system not been a common proper-motion pair. The estimates are extrapolated backward in time from the second-epoch astrometry, which for all except HD 129333 was obtained with NIRC2 on Keck and was more accurate, assuming proper motions from *Hipparcos* (Perryman et al. 1997) for HD 49197 and HD 129333 and from Tycho 2 (Høg et al. 2000) for V522 Per and RX J0329.1+0118. Parallactic motions were also taken into

TABLE 3
IR MAGNITUDES AND COLORS OF THE COMPANIONS

Object	ΔJ	ΔH	ΔK_S	$J - H$	$H - K_S$	K_S	$K_S - L'$
HD 49197B	9.6 ± 1.2	8.52 ± 0.12	8.22 ± 0.11	1.2 ± 1.2	0.33 ± 0.20	14.29 ± 0.14	...
HD 49197"C"	6.86 ± 0.10	6.82 ± 0.09	6.68 ± 0.10	0.27 ± 0.14	0.17 ± 0.14	12.75 ± 0.10	...
HD 129333B	3.38 ± 0.10	3.13 ± 0.09	3.04 ± 0.08	0.55 ± 0.14	0.19 ± 0.12	8.95 ± 0.08	...
V522 PerB	5.69 ± 0.09	5.44 ± 0.09	5.16 ± 0.09	0.63 ± 0.13	0.38 ± 0.13	14.51 ± 0.09	0.15 ± 0.18
RX J0329.1+0118B	4.22 ± 0.12	3.86 ± 0.08	3.65 ± 0.08	0.59 ± 0.15	0.31 ± 0.13	12.85 ± 0.09	...

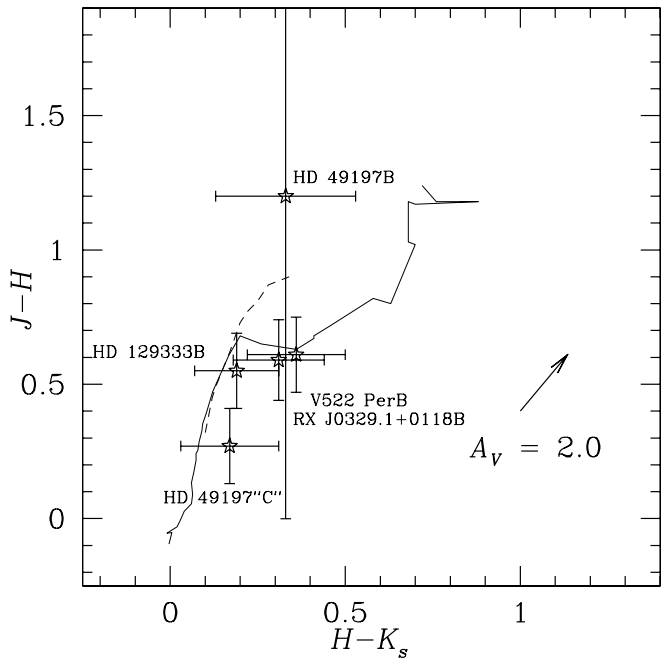

FIG. 5.—Near-IR color-color diagram of the detected companions. The solid line represents the B2 V–L8 V main sequence, with data compiled from Cox (2000; B2 V–M6 V) and Kirkpatrick et al. (2000; M8 V–L8 V). The dashed line shows the G0–M7 giant branch (Cox 2000). The Cox (2000) and Kirkpatrick et al. (2000) colors are converted from the Johnson-Glass (Bessell & Brett 1988) and 2MASS (Cutri et al. 2003) systems, respectively, to the CIT system using relations from Carpenter (2001). HD 49197"C" is too blue to be a bona fide low-mass companion to HD 49197. The near-IR colors of the remainder of the companions agree well with their inferred spectral types (Table 6).

account, as they are significant for stars $\lesssim$200 pc at our astrometric precision (several milliarcseconds). The assumed proper motions and parallaxes for all stars are listed in Table 2. To ensure the correct propagation of astrometric errors, the epoch transformations were performed following the covariant treatment of the problem, as detailed in Lindegren (1997).

Proper-motion diagrams for each object are presented in Figures 6–8. The first- and second-epoch measurements are shown by filled circles with error bars, and the inferred first-epoch position (assuming noncommon proper motion) is shown only with error bars. The dashed line reflects the combined proper and parallactic motion of the primary over the period between the two epochs. Below we discuss the evidence for common proper motion in each system.

3.2.1. *HD 49197*

The existence of the close (0.″95) companion to HD 49197 was unappreciated prior to the second-epoch imaging: the star was followed up because of the more distant (6.″8) candidate companion (HD 49197"C"). Upon its discovery in the Keck image (Fig. 1*c*), the close companion was recovered in the earlier Palomar image, where a dark circular ring around the core at the radial distance of the first Airy null ($\approx$0.″1) distinguishes it from the telescopic speckles (Fig. 1*b*).

As is evident from Figure 6, HD 49197B (*left panel*) is much more consistent with being a proper-motion companion of the primary than with being an unrelated background star projected along the same line of sight, whereas the reverse holds for HD 49197"C" (*right panel*). Therefore, we claim that the close-in HD 49197B is a bona fide companion, whereas the more widely separated HD 49197"C" is not.

The astrometry for HD 49197B from the two observational epochs is not in perfect agreement, perhaps because of its orbital motion around component A. At a projected separation of 43 AU, the orbital period will be greater than 240 yr (assuming a circular face-on orbit and a mass of 1.16 $M_\odot$ for the F5 V primary; Allende Prieto & Lambert 1999), resulting in a change in position angle of less than 2.°6 between the two epochs. This may explain the observed discrepancy of 0.°64 $\pm$ 0.°47 in position angle between the two observations, while the change in separation (2.4 $\pm$ 5.8 mas) is consistent with being zero. Future observations spanning a sufficiently long time line may be used to determine the dynamical mass of the HD 49197A/B system.

3.2.2. *HD 129333*

The offset positions of the companion to HD 129333 in the two observations taken 16 months apart are fully consistent with each other and inconsistent with the object being a background star (Fig. 7). HD 129333B thus shares the proper motion of the primary and is a bona fide companion.

3.2.3. *V522 Per and RX J0329.1+0118*

The astrometry for these two systems (Fig. 8) is inconclusive because of their smaller proper motions, insufficient time span between the observations, and/or less accurate astrometry. The likelihood of physical association of the companions with the primaries is investigated from low-resolution spectroscopy in § 4.1.

3.3. *Spectroscopy*

Infrared spectral classification of M–L dwarfs is done most successfully in the *J* and *H* bands, where a suite of indices based on the relative strengths of H_2O, FeH, K I, and Na I absorption has been developed to characterize their effective temperatures (Slesnick et al. 2004; Geballe et al. 2002; Gorlova et al. 2003; McLean et al. 2003) and surface gravities (Gorlova et al. 2003). However, spectroscopy of cool companions in the bright halos of their primaries is often more difficult at *J* and *H* than at *K* because of larger flux contrast and poorer quality of

TABLE 4
ASTROMETRY OF THE COMPANIONS

	Epoch 1		Epoch 2		Epoch 1 (If Noncommon Proper Motion)	
Object	Offset (arcsec)	P.A. (deg)	Offset (arcsec)	P.A. (deg)	Offset (arcsec)	P.A. (deg)
HD 49197B.....	0.9499 $\pm$ 0.0054	78.25 $\pm$ 0.40	0.9475 $\pm$ 0.0022	77.60 $\pm$ 0.25	0.9029 $\pm$ 0.0037	81.87 $\pm$ 0.31
HD 49197"C"	6.971 $\pm$ 0.030	346.13 $\pm$ 0.34	7.016 $\pm$ 0.008	346.50 $\pm$ 0.10	6.950 $\pm$ 0.009	346.10 $\pm$ 0.10
HD 129333B.....	0.7343 $\pm$ 0.0032	173.19 $\pm$ 0.35	0.7363 $\pm$ 0.0032	173.37 $\pm$ 0.35	0.7221 $\pm$ 0.0033	180.68 $\pm$ 0.37
V552 PerB	2.0970 $\pm$ 0.0090	194.02 $\pm$ 0.34	2.0937 $\pm$ 0.0032	193.91 $\pm$ 0.11	2.0991 $\pm$ 0.0032	193.93 $\pm$ 0.11
RX J0329.1+0118B	3.75 $\pm$ 0.05	303 $\pm$ 5	3.781 $\pm$ 0.016	303.85 $\pm$ 0.34	3.714 $\pm$ 0.070	303.7 $\pm$ 1.1

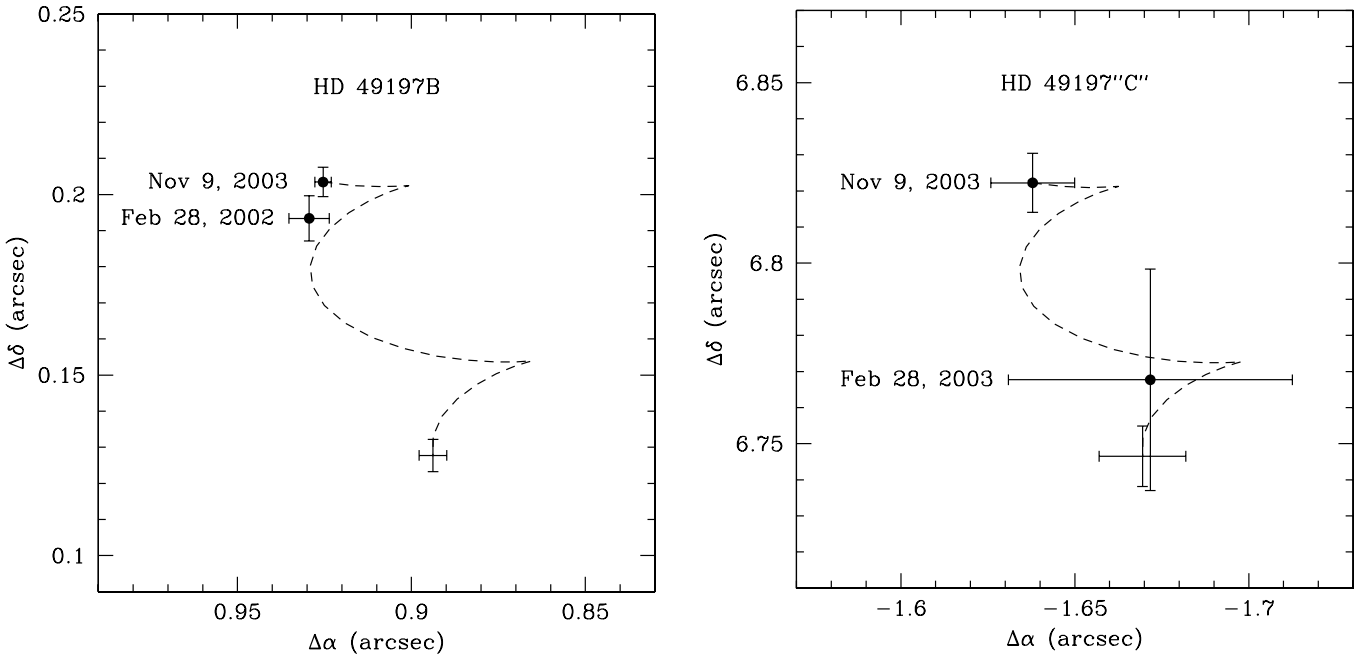

FIG. 6.—Proper-motion diagram for the two companions to HD 49197. The offsets from the primary at each observational epoch are plotted by filled circles with error bars. The inferred offsets at the first epoch (assuming noncommon proper motion) are shown just with error bars. The dashed lines reflect the proper and parallactic motions of the primary between the two epochs. HD 49197B is a common proper-motion companion within the 1 σ errors, while HD 49197"C" is more consistent with being a background object.

the AO correction at shorter wavelengths. Here we present *J*-band spectra of the two brighter companions: HD 129333B and V522 PerB. Cool dwarfs can be classified at *K* band based on the strength of their H_2O absorption shortward of 2.05 μm, the depth of the CO 2.29 μm band head, and the equivalent width (EW) of the Na I 2.21 μm doublet (Kleinmann & Hall 1986; Ali et al. 1995; McLean et al. 2003; Slesnick et al. 2004). Even cooler, late L and T dwarfs are best characterized by the strength of their CH_4 absorption at greater than 2.20 μm (Burgasser et al. 2002; McLean et al. 2003). We present *K*-band spectra of all four companions discussed in this paper.

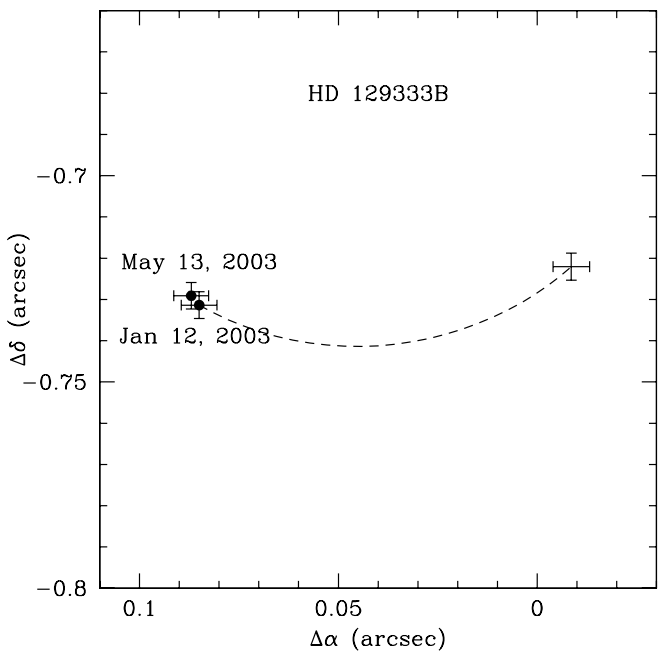

FIG. 7.—Same as Fig. 6, but for the companion to HD 129333. Within the 1 σ errors, the companion shares the proper motion of the primary.

Spectral types of the detected companions have been determined following infrared absorption line classification systems at *K* band (for Na I, Ca I, and CO) from McLean et al. (2003; spectral types M6 V–T8) and Ali et al. (1995; F3 V–M6 V) and at *J* band (for K I and Ti I) from Gorlova et al. (2003; M4 V–L8) and Wallace et al. (2000; O7–M6). Luminosity classes are based on the relative strengths of Na I, Ca I, and CO absorption at *K* band (Kleinmann & Hall 1986) and on the strengths of Mn I and K I absorption at *J* (Wallace et al. 2000; Gorlova et al. 2003).

We have avoided the use of temperature-sensitive H_2O indices that span large fractions of the spectrum ($\gtrsim$4% total bandwidth, e.g., the H_2OD index of McLean et al. 2003, or the H_2O-2 index of Slesnick et al. 2004) because of their strong dependence on the overall continuum shape of the spectrum and because of the uncertainties in the spectral shapes of faint companions extracted from the halos of bright objects (§ 2.3). We have used the *J*-band 1.34 μm H_2O index of Gorlova et al. (2003), however, which measures only the onset of H_2O absorption at that wavelength and is narrow (1.4% bandwidth).

Below we analyze the *K*- and *J*-band spectra of the companions to HD 49197, HD 129333, V522 Per, and RX J0329.1+0118. The inferred effective temperatures and spectral types are provided in Tables 5 and 6.

3.3.1. *K-Band Spectroscopy of HD 49197B*

Our spectrum of HD 49197B (Fig. 3) shows strong CO and H_2O bands characteristic of ultracool dwarfs but lacks a CH_4 absorption feature, indicating that it is earlier than L8 (Geballe et al. 2002). On the other hand, Na I absorption is also absent from the spectrum, pointing to a spectral type of L3 or later (McLean et al. 2003), independent of gravity (cf. Fig. 8 in Gorlova et al. 2003). Following the analysis of $R \sim 2000$ *K*-band spectra of M6–T8 dwarfs in McLean et al. (2003), we form a CO absorption index from the ratio of the median flux in an absorbed (2.298–2.302 μm) versus an unabsorbed (2.283–2.287 μm) region of the spectrum. We find CO $= 0.80 \pm 0.03$

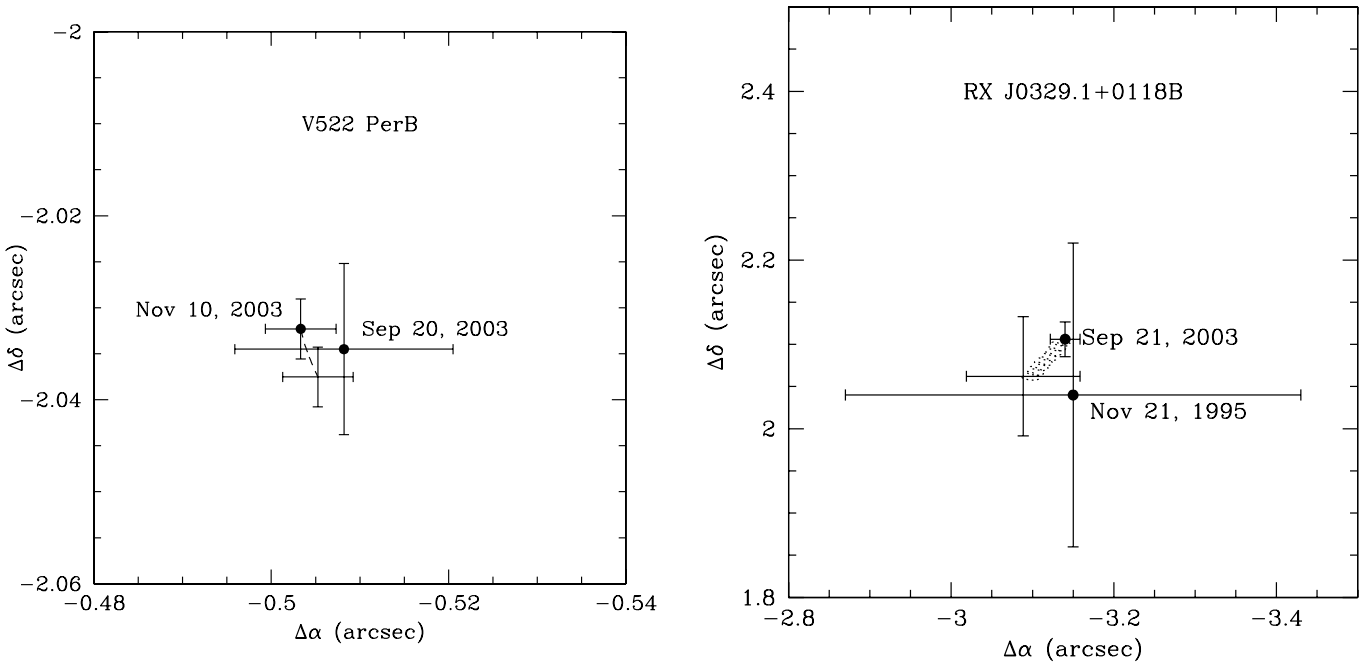

FIG. 8.—Same as Fig. 6, but for the companions to V522 Per (*left*) and RX J0329.1+0118 (*right*). The 1995 November 21 data point for the companion to RX J0329.1+0118 is from Sterzik et al. (1997) and is set to be at the mean epoch of their observations (1995 November 19–23). The proper motions of the primaries between the observation epochs are too small to decide the physical association of the companions within the astrometric errors. The probability of association in each system is estimated from near-IR spectroscopy (§ 4.1).

(where the error has been estimated as the quadrature sum of the relative uncertainties of the median in the two spectral regions), which indicates a spectral type of L7 or later. However, the CO index is not very sensitive to L dwarf temperatures and varies by up to 0.15 (60% of its total range of variation between spectral types M5 and T2) within the same spectral type (Fig. 13 in McLean et al. 2003).

Alternatively, we can also use the absolute K_S-band magnitude of HD 49197B to estimate its spectral type, following the empirical relation of Kirkpatrick et al. (2000), based on a sample of 24 M and L dwarfs with measured parallaxes:

$$M_{K_S} = 10.450 + 0.127(\text{subclass}) + 0.023(\text{subclass})^2, \qquad (1)$$

where subclass $= -1$ for M9 V, 0 for L0 V, 1 for L1 V, etc. The scatter about the fit is approximately one subclass. From the inferred apparent K_S magnitude of HD 49197B and from the parallax of the primary, we obtain $M_{K_S} = 11.04 \pm 0.24$ for the secondary, which corresponds to a spectral type of L3 $\pm$ 1.5.

We assign a final spectral type of L4 with an uncertainty of one subclass. This is based on the intersection of the results from our spectroscopic analysis, suggesting L3–L7, and from the K_S-band absolute magnitude, pointing to L1.5–L4.5. A spectral type of L4 $\pm$ 1 for HD 49197B is also consistent with a by-eye comparison of its K-band spectrum with the grid of L dwarf standards from Leggett et al. (2001).

3.3.2. *K-Band Spectroscopy of HD 129333B, RX J0329.1+0118B, and V522 PerB*

We classify the K-band spectra of these companions following the analyses of Ali et al. (1995) and Kleinmann & Hall (1986), whose data are taken at similar resolutions to ours ($R = 1380$–3900 and 2500–3100, respectively) and span the F8–M7 spectral type range. We employ the spectral classification sequence of Ali et al. (1995), whose empirically derived indices are based on a larger sample of dwarf stars than in Kleinmann & Hall (1986).

Our reduced spectra were first shifted to 0 km s^{-1} heliocentric velocity, where the shift was determined by fitting Gaussian

TABLE 5
SPECTROSCOPIC MEASUREMENTS FOR THE COMPANIONS

Star	EW(Na I)[a] (Å)	EW(Ca I)[a] (Å)	EW(CO)[a] (Å)	EW(K I)[b] (Å)	H_2O Index[b]	$T_{\rm eff,Ca}$[c] (K)
HD 49197B	-0.3 ± 0.6	0.2 ± 0.4	0.82 ± 0.05[d]	...	...	<3000
HD 129333B	5.17 ± 0.59	4.79 ± 0.64	7.26 ± 0.57	2.18 ± 0.11	...	3660
V522 PerB	5.87 ± 0.58	3.11 ± 0.50	5.67 ± 0.38	1.07 ± 0.16	0.91 ± 0.01	3200
RX J0329.1+0118B	6.76 ± 0.60	3.81 ± 0.39	8.63 ± 0.17	...	...	3300

[a] At K band as defined by Ali et al. (1995).
[b] At J band as defined by Gorlova et al. (2003).
[c] Calculated from empirical relations relating $T_{\rm eff}$ to EW(Ca I) (Table 4 in Ali et al. 1995). The sign of the linear coefficient in the Ca I "cool" relation of Ali et al. (1995) has been changed from negative (as erroneously listed in their paper) to positive to match the slope of their empirical data. Ali et al. (1995) quote an error of $\pm$300 K for this index.
[d] The CO index for HD 49197B is not in Å, but as defined by McLean et al. (2003).

TABLE 6
ESTIMATED PROPERTIES OF THE COMPANIONS

Objects	Spectral Type	Mass ($M_\odot$)	Projected Separation (AU)	Probability of Chance Alignment
HD 49197B.....	L4 ± 1[a]	$0.060^{+0.012}_{-0.020}$	43	3×10^{-6}
HD 129333B.....	M2 ± 1[b]	$0.20^{+0.30}_{-0.08}$	25	3×10^{-6}
V522 PerB	M4 ± 1[b]	0.125 ± 0.025	400	2×10^{-3}
RX J0329.1+0118B	M3 ± 2[b]	$0.20^{+0.30}_{-0.10}$	380	9×10^{-4}

[a] Inferred from the *K*-band spectrum and from the absolute magnitude of the object (§ 3.3.1).
[b] Based on the estimate of the Ca I–derived effective temperature (Table 5) and on the *J*-band K I and H_2O absorption (if available). An MK spectral type vs. $T_{\rm eff}$ classification for dwarfs is adopted from Bessell (1991).

profiles to the Na I doublet and comparing the fitted line centers to their values in the solar spectrum (Mohler 1955). For consistency with the Ali et al. (1995) spectral classification, we have chosen the same bands for integrating the Na I (2.21 μm), Ca I (2.26 μm), and ^{12}CO(2–0) (2.29 μm) absorption. The continuum in the target spectra was fitted to three regions devoid of absorption lines: 2.0907–2.0951, 2.2140–2.2200, and 2.2873–2.2925 μm. These have been selected as a combination of the continuum regions used by Ali et al. (1995) and Kleinmann & Hall (1986), so as to constrain the fit on both sides of the Na I doublet (as in Kleinmann & Hall 1986, where the continuum-fitting regions are widely separated from the Na I lines), as well as near it (as in Ali et al. 1995, where the continuum is constrained only on the long-wavelength side of the Na I lines).

The absorption strength in each band was obtained as an equivalent width, by integrating the profile of the spectrum in the band with respect to a global continuum level defined by the three continuum bands. The only exception is the EW of the ^{12}CO(2–0) first-overtone band head, for which we have adopted the mean continuum level of the third continuum band (as in Kleinmann & Hall 1986 and Ali et al. 1995). The 1 σ errors in the EWs were calculated by propagating the rms noise of the spectrum in the nearest continuum band, assuming independent pixel variances. The EWs of Na I and Ca I were corrected for corresponding absorption in the spectra of the telluric standards, the EW of which (0.84 ± 0.57 Å for Na I and 1.14 ± 0.36 Å for Ca I in G stars; Ali et al. 1995) was added to that measured for the companions. The final EWs are listed in Table 5.

To infer effective temperatures for the companions to HD 129333, RX J0329.1+0118, and V522 Per, we employ empirical relations between the strength of *K*-band Na I, Ca I, and CO absorption and effective temperature ($T_{\rm eff}$), as determined by Ali et al. (1995; their Table 4). Na and CO produce the most characteristic *K*-band features of cool stars. However, their absorption strengths are inaccurate tracers of temperature for stars cooler than 4000 K and are, in addition, gravity sensitive (Kleinmann & Hall 1986; Gorlova et al. 2003). On the other hand, Ca I transitions in the *K* band require the population of higher energy states and hence are more temperature sensitive. However, their absorption strength is degenerate with the stellar effective temperature: Ca I absorption at 2.26 μm peaks at ~3500 K and decreases for higher and lower effective temperatures (Kleinmann & Hall 1986; Ali et al. 1995). This behavior is fitted via two separate $T_{\rm eff}$ versus EW(Ca I) relations in Ali et al. (1995). By combining the information from Ca I with that from Na I and ^{12}CO(2–0), we can break this degeneracy and use the more temperature-sensitive Ca I index to constrain the effective temperature for each star to within ~300 K (the quoted uncertainty of the Ca I index in Ali et al. 1995). For HD 129333B, with a Ca I absorption strength near the breaking point between the "hot" and "cool" relations, we take the average of the two estimates. For V522 PerB and RX J0329.1+0118B, whose Na I and CO absorption is indicative of temperatures $T_{\rm eff} < 3400$ K, we use only the "cool" relation. The effective temperatures inferred from Ca I absorption are listed in Table 5. As in Ali et al. (1995), we adopt a spectral type versus effective temperature classification for M dwarfs from Bessell (1991) and obtain spectral types of M1, M3, and M4 for HD 129333B, RX J0329.1+0118B, and V522 PerB, respectively, with an uncertainty of two spectral subtypes. A visual inspection and comparison of the strengths of the various absorption features with *K*-band spectral sequences from Leggett et al. (2001) and Wallace & Hinkle (1997) confirm these results. Given the comparable values of their Na I and ^{12}CO(2–0) EWs, all stars have likely dwarf gravities (cf. Fig. 7 in Kleinmann & Hall 1986).

3.3.3. *J-Band Spectroscopy of HD 129333B and V522 PerB*

We further constrain the spectral types of HD 129333B and V522 PerB from their *J*-band spectra. These show the characteristic absorption features of M stars: K I lines at 1.169, 1.177, 1.243, and 1.252 μm, Fe I at 1.188 and 1.197 μm, Na I at 1.268 μm, Al I at 1.312 and 1.315 μm, and H_2O absorption at $\lambda > 1.34$ μm (Fig. 4). The spectrum of V522 PerB exhibits also Ti I and Mn I absorption over 1.282–1.298 μm. Spectral classification at *J* band was done based on the depth of the H_2O and K I absorption, following the index definitions of Gorlova et al. (2003). After resampling our data to match the $R \approx 350$ spectral resolution of Gorlova et al. (2003), we form the 1.34 μm water index as the ratio of the mean fluxes (in a 0.004 μm wide region) at 1.336 and 1.322 μm, and we measure the K I EW by integrating the absorption over the region 1.2375–1.2575 μm. Because K I absorption in the solar-like photospheres of the telluric standards is small [EW(K I λ1.14 μm) ≈ 0.1EW(Na I λ2.21 μm) = 0.08 Å for the Sun; Mohler 1955; Ali et al. 1995], the K I EW measurements of the companions were not corrected for it.

For HD 129333B, we cannot estimate the strength of the 1.34 μm water absorption because of insufficient spectral coverage. The EW of K I indicates a spectral type of M2–M4. Averaging this with our *K*-band estimate of M1 ± 2, we assign a spectral type of M2 ± 1 for HD 129333B. Given the youth of HD 129333 (<120 Myr; see § 4.2), the companion may have lower than dwarf gravity. The effect of this on alkali absorption lines in the near-IR is degenerate with temperature (Gorlova et al. 2003; McGovern et al. 2004) and could be compensated by a later spectral type. However, spectral types later than M3 are inconsistent with the depth of the strongly temperature-sensitive Ca I absorption in this star (§ 3.3.2). In addition,

HD 129333B lacks noticeable Mn I absorption, which is weak in M dwarfs but grows deeper with decreasing surface gravity in M stars (Fig. 9 in Wallace et al. 2000). Hence, we conclude that HD 129333B is an M2 $\pm$ 1 dwarf.

For V522 PerB, both the K I EW and the water absorption index point to a spectral type of M3–M5, in agreement with our *K*-band estimate (M4 $\pm$ 2). The stronger Ti I absorption than in HD 129333B is also consistent with a cooler photosphere. We thus assign a spectral type of M4 $\pm$ 1 to V522 PerB. The strength of the Mn I transition indicates a potentially subgiant surface gravity, although as noted in § 3.3.2, the effect is not seen at *K* band.

4. DISCUSSION

4.1. *Likelihood of Physical Association*

Our astrometric follow-up of HD 49197B and HD 129333B confirmed common proper motion between these two companions and their respective primaries. However, the smaller proper motions of V522 Per and RX J0329.1+0118 prevented us from concluding the same for their respective companions, given the time span of our observations. The probability of physical association in these systems can be inferred from the spectroscopically determined spectral types and absolute magnitudes of the companions. If the absolute magnitude inferred from the spectral type of a companion agrees with its measured apparent magnitude at the heliocentric distance of the respective primary, then the companion is likely to be a bona fide one (modulo the space density of stars of similar spectral type as the companion).

Figure 9 presents a comparison of the spectroscopic versus photometric absolute magnitudes. The correspondence is good for the four companions followed up via near-IR spectroscopy, indicating that they are at similar heliocentric distances as their primaries and are thus likely to be physically bound to them. The location of the remaining candidate companion (HD 49197"C") along the ordinate is inferred from its near-IR colors. As mentioned in § 3.1, HD 49197"C" is a likely F–G star ($2.0 \leq M_K \leq 4.0$; Cox 2000); i.e., it is intrinsically too bright to be associated with HD 49197 (F5 V) given its faint apparent magnitude.

A robust statistical analysis of the likelihood of chance alignment in the four systems discussed here is not yet possible at this stage of the survey. They are only a fraction of the ones discovered to have candidate companions. With follow-up observations still in progress, the exact number of bound systems is unknown. We defer a discussion of the companion chance alignment probability based on the full ensemble statistics until a later paper. Here we consider these probabilities only on a per system basis. To give an approximate idea of the limited statistics from which these preliminary results are extracted, we point out that to date we have analyzed multiepoch astrometric data for approximately 15 stars (mostly from the deep survey) with faint ($\Delta K_S > 3$, i.e., expected to be of spectral type M or later) companions within 4″.

We base our calculation of the probability of false association in each system on the empirically determined spatial density of cool objects (M–T spectral types) in the solar neighborhood. There are 112 such known objects in the northern ($\delta > -20^\circ$) 8 pc sample (Reid et al. 2003). The northern 8 pc sample covers 65% of the sky and is estimated to be ~15% incomplete. The total number of cool objects and white dwarfs within 8 pc of the Sun is therefore expected to be 198, with a volume density of 0.10 pc^{-3}. This estimate is based on a small fraction of the thin-disk population (scale height 325 pc; Bahcall & Soneira 1980) of the Galaxy and hence should not vary substantially as a function of Galactic latitude.

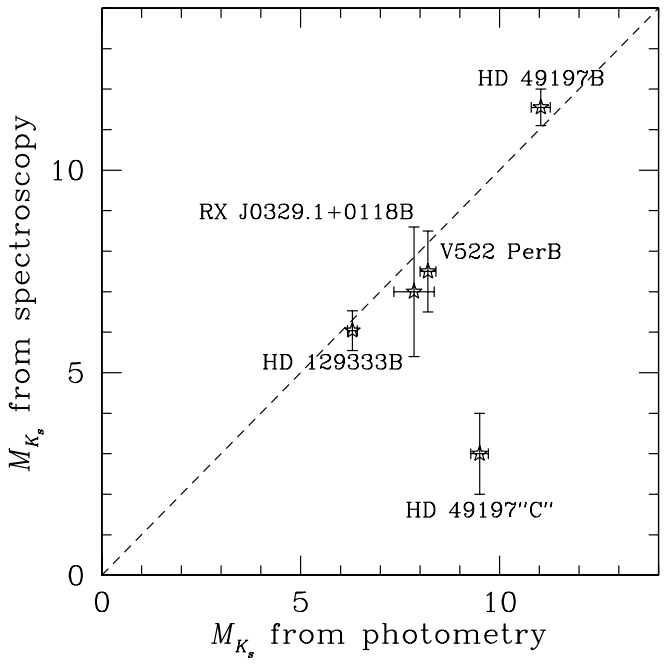

FIG. 9.—Comparison of the photometrically derived absolute K_S-band magnitudes of the companions (assuming the heliocentric distances of the corresponding primaries) to the spectroscopically inferred ones. The dashed line has a slope of unity. The location of HD 49197"C" (of which no spectra were taken) along the vertical axis is based on a spectral type (F–G) inferred from its near-IR colors (§ 3.1). HD 49197"C" is intrinsically too bright to be at the same heliocentric distance as HD 49197, whereas the remainder of the companions are consistent with being at the distances of their respective primaries.

We then calculate the number of cool dwarfs expected to be seen in projection toward each system within a conical volume of radius 4″ centered on the star, with the observer at the apex of the cone. We truncate the radial extent of the conical volume by requiring that the apparent *K* magnitude of a projected companion falls within the limits allowed by the spectral type (and hence absolute magnitude) of the detected one. Absolute *K* magnitudes for the M2–M4 dwarfs discussed here have been adopted from Bessell (1991). Although Bessell's M dwarf classification system predates the discovery of ultracool dwarfs (later than M5), it remains valid for early M dwarfs. For L4 $\pm$ 1 spectral types we adopt absolute *K* magnitudes from Dahn et al. (2002).

The expected number μ of unrelated cool dwarfs within the relevant volume around each star is listed in the last column of Table 6. Given that for all stars $\mu \ll 1$, we can assume that the event of seeing an unrelated field object in the vicinity of one of our program stars is governed by Poisson statistics. Hence, the probability of finding one or more such dwarfs near any given star (i.e., the probability of chance alignment) is $1 - e^{\mu} \approx \mu$. As seen from Table 6, after having followed up the companions spectroscopically, we can claim with $\geq$99.99% certainty in each case that the companion is physically associated with its respective primary. As discussed above, such probabilities need to be regarded in the context of the ensemble statistics. Within our sample of four spectroscopically confirmed companions, the probability that at least one is a false positive is 3×10^{-3}. This exemplifies the power of spectroscopic follow-up as an alternative to multiepoch astrometry in constraining the likelihood of physical association in a system.

4.2. *Stellar Ages and Companion Masses*

We estimate the ages of the primaries (Table 2) from published data on their chromospheric activity, Li I equivalent width, and kinematic association with young moving groups. Masses for each of the companions (Table 6) were determined from either the low-mass pre–main-sequence evolutionary models of Baraffe et al. (1998) or the brown dwarf cooling models of Chabrier et al. (2000; "DUSTY") and Burrows et al. (1997). We have not used the dust-free "COND" models of Baraffe et al. (2003), since they are more appropriate for temperatures $\lesssim$1300 K (i.e., for T dwarfs) when all grains are expected to have gravitationally settled below the photosphere.

HD 49197B.—From the strength of Ca H and K core emission in Keck HIRES spectra of the primary, Wright et al. (2004) determine an age of 525 Myr for HD 49197, which we assume to be accurate to within $\approx$50%, given the variation in chromospheric activity of solar-type stars (Henry et al. 1996). No other age-related indicators exist in the literature for this F5 star. From our own high-resolution optical spectra, we measure EW(Li λ6707.8) = 80 mÅ (L. A. Hillenbrand et al. 2004, in preparation), consistent with a Pleiades-like (120 Myr; Stauffer et al. 1998) or older age. Hence, we adopt an age of 260–790 Myr for the primary. Assuming coevality, the mass of the secondary is $0.060^{+0.012}_{-0.025}$ $M_\odot$ (Burrows et al. 1997; Chabrier et al. 2000), where the range of masses accommodates the 1 σ error in the inferred absolute magnitude of the secondary and the allowed age range for the primary. HD 49197B is thus a brown dwarf.

HD 129333B.—The primary is a well-known young star, kinematically belonging to the Local Association (Pleiades moving group, 20–150 Myr; Soderblom & Clements 1987; Montes et al. 2001b). Results from the Mount Wilson spectroscopic survey (Soderblom 1985) and from the Keck/Lick r.v. program (Wright et al. 2004) show strong Ca II H and K emission, indicating high levels of chromospheric activity and youth. Wright et al. (2004) list an age of less than 10 Myr for this star, although the chromospheric activity-age relation is not reliable for stars that young, in part because of the large variance in rotation rates of stars younger than 50–80 Myr (e.g., Soderblom et al. 1993) and because the relation is not calibrated at such young ages. Montes et al. (2001a) report strong Li I absorption [EW(Li I) = 198 mÅ] and conclude that the star is "significantly younger" than the Pleiades (120 Myr; Stauffer et al. 1998). Assuming an age of 10–100 Myr for the system, we estimate the mass of the secondary at $0.20^{+0.30}_{-0.08}$ $M_\odot$ (from models of Baraffe et al. 1998).

V522 PerB.—The primary is a member of the α Per open cluster, confirmed by photometry, kinematics, and spectroscopy (Prosser 1992). From high-resolution spectroscopy and determination of the lithium depletion boundary in the cluster, Stauffer et al. (1999) determine an age of 90 $\pm$ 10 Myr, consistent with a recent age estimate from upper main-sequence turnoff fitting (Ventura et al. 1998). Using the Lyon group stellar evolution models (Baraffe et al. 1998), we determine a mass of 0.085–0.15 $M_\odot$ for the secondary. However, from their substellar "DUSTY" code (Chabrier et al. 2000), the treatment of dust opacity in which may be more appropriate for this cool ($\sim$3200 K) star, we find that its mass is $\geq$0.10 $M_\odot$. We thus estimate 0.10–0.15 $M_\odot$ for the mass of V522 PerB.

RX J0329.1+0118B.—Neuhäuser et al. (1995) list RX J0329.1+0118 (G0 IV) as a fast-rotating ($v \sin i = 70$ km s^{-1}) X-ray source south of Taurus, with an Li I equivalent width of 110 mÅ—all indicators of relative youth. Assuming a common origin and distance with the stars in the Taurus molecular cloud (140 pc; Kenyon et al. 1994), the authors claim that its bolometric luminosity is higher than that of a zero-age main-sequence star, and the star is therefore likely in the pre–main-sequence phase. From a proper-motion survey of pre–main-sequence stars in Taurus-Auriga, however, Frink et al. (1997) find that the young stars south of Taurus discussed in Neuhäuser et al. (1995) are kinematically unrelated to those in Taurus and that star formation in the two complexes must have been triggered by different events. From the Pleiades-like Li I equivalent width of RX J0329.1+0118, we assign an age of $\approx$120 Myr for this star. Given the spectral type of the secondary, its mass is $0.20^{+0.30}_{-0.10}$ $M_\odot$ (Baraffe et al. 1998).

4.3. *HD 129333: Binary or Triple?*

The existence of a stellar companion to HD 129333 has already been inferred in the r.v. work of Duquennoy & Mayor (1991, hereafter DM91), who find that the star is a long-period single-lined spectroscopic binary (SB1). From their derived orbital parameters, the authors determine a secondary mass $M_2 \geq 0.37$ $M_\odot$ and suggest that the star be targeted with speckle interferometry to attempt to resolve the companion. We should therefore consider whether the companion that we have resolved (and named HD 129333B) is identical to the spectroscopically inferred one.

4.3.1. *The Combined Radial Velocity and Astrometric Solution*

Combining r.v. and astrometric data presents a powerful approach to fully constrain all the orbital elements of a binary system. In this section we test the hypothesis that the DM91 and the imaged companions are identical by attempting to solve for the parameters of the relative orbit and checking for consistency with all available data.

The orbital parameters that can be determined through r.v. monitoring of an SB1 are the eccentricity e, the period P, the epoch T_0 of periastron, the longitude ω of periastron, the systemic radial velocity $v_{\mathrm{rad},0}$, and the primary velocity semiamplitude K_1. K_1 is related to the other orbital parameters through the mass function

$$f(M) = \frac{(M_2 \sin i)^3}{(M_1 + M_2)^2} = \frac{(1 - e^2)^{3/2} P K_1^3}{2\pi G}, \qquad (2)$$

where $M_{1,2}$ are the component masses, i is the inclination of the orbit with respect to the observer, and π and G are constants (e.g., Heintz 1978, p. 80). The orbital inclination i cannot be constrained from r.v. monitoring; hence, the masses and the semimajor axes $a_{1,2}$ of the binary components are degenerate with i.

From astrometric observations we can fit for e, P, T_0, ω, i, $a_{1,2}$ (and hence $M_{1,2}$), and the only remaining parameter, i.e., the longitude of the ascending node Ω. Therefore, by performing a least-squares fit to the combined and appropriately weighted r.v. and astrometric data, one can fully determine the orbit of a binary and attain greater precision in estimating the orbital elements (Morbey 1975).

We first list the orbital parameters that have been already determined. Based on the r.v. measurements shown in Figure 10, DM91 find $e = 0.665 \pm 0.023$, $T_0 = \mathrm{JD}\ 2{,}446{,}932 \pm 20 =$ year 1987.37, $\omega = 188\overset{\circ}{.}0 \pm 5\overset{\circ}{.}2$, $K_1 = 5.09 \pm 0.20$ km s^{-1}, and $P = 4575$ days $= 12.53$ yr. DM91 state, however, that the period is probably accurate only "to the nearest unit of log P" (i.e., $10^{3.5}$ days $< P < 10^{4.5}$ days, or between 8.7 and 87 yr) and calculate the uncertainties in e, T_0, ω, and K_1 for a fixed P. Nevertheless, because of the high eccentricity of the orbit and

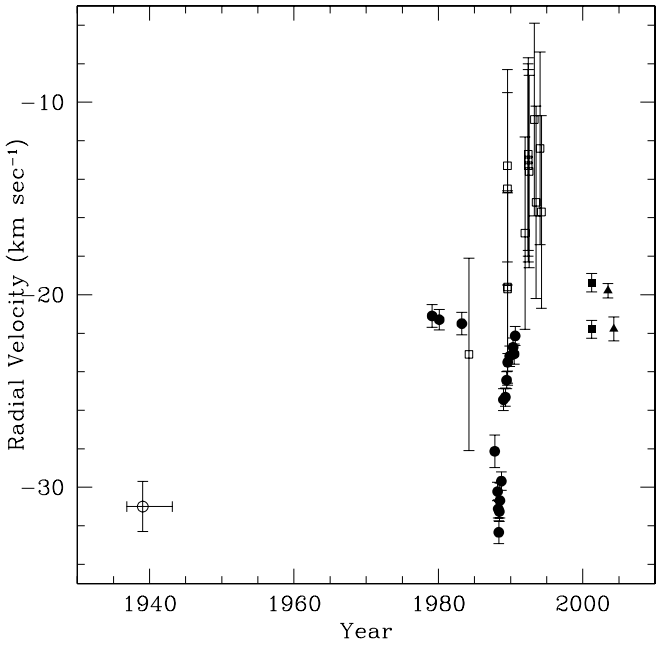

FIG. 10.—Radial velocity data for HD 129333 from the literature. Data from DM91 are plotted by filled circles, from Dorren & Guinan (1994) by open squares, from Montes et al. (2001a) by filled squares, and from Wilson & Joy (1950) by an open circle. Our own unpublished r.v. data are shown by filled triangles. The exact epoch of the Wilson & Joy (1950) observation is unknown. Given the DM91 orbital solution and the current phase coverage, periods of less than 16 yr can be excluded.

because of their adequate observational coverage of the star near r.v. minimum, the final values of these three parameters are not expected to be significantly different. Assuming that the r.v. and the resolved companions are the same, we impose the additional constraints derived from our astrometric observations, namely, the separation ρ and position angle ϕ between the binary components on 2003 May 13 (T = JD 2,452,772 = year 2003.36). Given the long (multiyear) orbital period and the small change (insignificant within the error bars) between our two relative astrometric observations taken 4 months apart, we only use one of the astrometric measurements. Finally, we adopt a mass of 1.05 $M_\odot$ for the G0 V primary, based on an estimate from Dorren & Guinan (1994).

The equation that determines the binary orbit is Kepler's equation:

$$E - e \sin E = \frac{2\pi}{P}(T - T_0), \tag{3}$$

where the eccentric anomaly E is related to the true anomaly θ through

$$\tan\frac{\theta}{2} = \left(\frac{1+e}{1-e}\right)^{1/2} \tan\frac{E}{2}. \tag{4}$$

The remaining equations are

$$P = 2\pi\sqrt{\frac{a^3}{G(M_1 + M_2)}}, \tag{5}$$

$$r = a(1 - e\cos E), \tag{6}$$

$$\rho^2 = r^2\left[1 - \sin^2(\theta + \omega)\sin^2 i\right], \tag{7}$$

$$\tan\Omega = \frac{\tan\phi - \tan(\theta + \omega)\cos i}{1 + \tan\phi\tan(\theta + \omega)\cos i}. \tag{8}$$

Because the orbital period of HD 129333 is poorly constrained by DM91, we choose to treat P as a free parameter. Thus, there are eight unknown parameters: P, M_2, i, a (the semimajor axis of the relative orbit), Ω, E, the radius vector $r(T - T_0)$, and the true anomaly $\theta(T - T_0)$ of the companion in the relative orbit at time $T - T_0$. From the combined imaging and r.v. data we have imposed seven constraints: $\rho(T - T_0)$, $\phi(T - T_0)$, e, ω, M_1, K_1, and $T - T_0$. Given that the number of unknowns is greater than the number of constraints, we cannot solve unambiguously for the parameters, let alone use a least-squares approach to determine their best-fitting values. However, by stepping through a grid of constant values for one of the parameters, we can determine the rest.

We choose M_2 as our step parameter for the grid, treating it as a known parameter. In principle, we can use equations (4)–(7) to express P in terms of M_2, E, and the known variables and then substitute this expression in equation (3), which can be solved for E. However, because of the complexity of the general functional form $P(M_2,\ E,\ \rho,\ \phi,\ e,\ \omega,\ M_1,\ K_1,\ T - T_0)$ and because Kepler's equation cannot be solved analytically, we employ a two-stage iterative approach. In the outer iteration, for a given value of M_2 we converge on a solution for P, and in the inner iteration we use the Newton-Raphson method to solve Kepler's equation for E. The iterative Newton-Raphson method has been described in detail elsewhere (e.g., Press et al. 1992), so we do not discuss it further. The convergence of the outer iteration loop, however, merits a brief description.

We take an initial estimate P_0 for the period and invert equation (2) to obtain a numerical value for $\sin i$ as a function of P and M_2. From equations (4)–(7) we then express P in terms of the known parameters plus M_2, E, and $\sin i$ and plug that expression into equation (3), which is then easier to solve for E. Once E is obtained, we invert Kepler's equation to find a solution $P = P_1$ for the orbital period that depends on the initial guess P_0. We repeat the above procedure by substituting P_1 for P_0 and so forth until the values P_j converge. We stop when the value of P is constrained to better than 0.1%, which usually occurs after three to four iterations. Because of the monotonic dependence of the orbital elements i, a, and E on P, we can be certain that the thus-obtained solution for P is unique.

Following the above procedure and adopting the DM91 values for e, T_0, and K_1, we find that if the resolved companion is identical to the r.v. one, its mass is at least 0.68 $M_\odot$, with a corresponding period of 50.0 yr, a = 16.3 AU, and $i = 85^\circ$. Values as small as M_2 = 0.58 $M_\odot$ (P = 42.8 yr, a = 14.4 AU, $i = 84^\circ$) are possible if all parameters are set at their 1 σ deviations that minimize M_2.

However, a minimum mass of $\approx$0.58 $M_\odot$ for HD 129333B does not agree with the constraint from our IR spectroscopy, $M_2 \leq 0.50\ M_\odot$ (§§ 3.3 and 4.2), obtained from comparison to theoretical evolutionary tracks from Baraffe et al. (1998). Moreover, a companion with mass $M_2 \geq 0.58\ M_\odot$ (spectral type K8 or earlier; Cox 2000) would be too bright in absolute magnitude ($M_K \leq 5.1$; Bessell 1991) to be identified with HD 129333B ($M_{K_S} = 6.30 \pm 0.12$, from its apparent magnitude and from the *Hipparcos* distance to HD 129333). It is therefore likely that the r.v. and spectroscopic companions are not identical.

The inconsistency between the masses could be explained by noting that a recent study of low-mass binaries by Hillenbrand & White (2004) has shown that most modern stellar evolutionary models tend to underestimate dynamical masses of main-sequence and pre–main-sequence stars. According to the authors, the Baraffe et al. (1998) models underestimate the mass of a 0.5 $M_\odot$ main-sequence star by $\approx$20%. This could reconcile

the limits on the mass of HD 129333B obtained from near-IR spectroscopy with those from the orbital solution. However, the problem of the companion being subluminous remains.

4.3.2. *Comparison to Other Radial Velocity Data*

The DM91 set of r.v. data is the most accurate and deterministic for the orbit of HD 129333. Other data exist from Wilson & Joy (1950), Dorren & Guinan (1994), Montes et al. (2001a), and our own high-resolution spectroscopic observations[3] (Fig. 10); however, they do not improve the orbital phase coverage greatly. Although Dorren & Guinan (1994; data plotted by open squares) appear to have captured the binary near an r.v. maximum around 1993, their data are less restrictive because of their large uncertainties. In addition, the Dorren & Guinan (1994) data for 1990 systematically overestimate the r.v. of the primary with respect to DM91 data taken over the same period. We therefore choose to disregard the Dorren & Guinan (1994) data set. The remaining data are very limited, and we do not attempt to use them to refit the DM91 orbital solution. However, they are of some utility in constraining the orbital period.

Because no other r.v. minimum is observed for HD 129333 between 1987.37 and 2003.36, we conclude that $P > 16$ yr. The Wilson & Joy (1950) data point (based on three measurements) is consistent with an r.v. minimum and is thus critical in constraining the orbital period. However, the authors do not list an epoch for the observations. The Wilson & Joy (1950) data were taken in the course of the Mount Wilson stellar spectroscopic survey and are kept in the Ahmanson Foundation Star Plates Archive.[4] After consultation with the original plates, we retrieve the dates of the individual observations: 1936 March 10 (year 1936.19), 1936 June 4 (year 1936.42), and 1942 June 24 (year 1942.48). We adopt the mean date of these observations, the year $1938.4^{+4.1}_{-2.2}$, as the epoch for the Wilson & Joy (1950) measurement $v_{\rm rad} = -31.0 \pm 1.3$ km s^{-1}, where the errors in the epoch correspond to the interval between their first and last observation. Because of its highly eccentric orbit, the star must have been within 1 yr of r.v. minimum at this epoch. Given the r.v. minimum in 1987.37 and $P > 16$ yr, we infer that the r.v. companion has a likely orbital period equal to the interval between the two observed minima or to some integer fraction thereof: $49.0^{+2.4}_{-4.2}$, $24.5^{+1.2}_{-2.1}$, or $16.3^{+0.8}_{-1.4}$ yr (all consistent with the DM91 estimate).

The 49 yr orbital period agrees with the one obtained in § 4.3.1 and supports the evidence that the r.v. and resolved companions may be identical. If the r.v. companion was on a 24.5 yr period ($a = 9.8$ AU, from the DM91 orbital elements), it would have been $\gtrsim 0\farcs33$–$0\farcs44$ from the primary during our imaging in 2003, with mass $M_2 \geq 0.47\ M_\odot$. Such a companion should have been at least as bright as the resolved one ($\Delta K_S = 3.0$), although it could have fallen just below our detection limits ($\Delta K_S \approx 3.0$ at $0\farcs4$) if it was at the lower limit of the allowed mass range. Given $q = M_2/M_1 \geq 0.46$ in this case, the star should be easily detectable as a double-lined spectroscopic binary (SB2) through high-resolution spectroscopy in the near-IR, where the contrast favors detecting SB2 systems with mass ratios as small as 0.2 (Prato et al. 2002). A 16.3 yr period can most probably be excluded, since the 2003 data point does not indicate an approaching r.v. minimum (Fig. 10) in late 2003–2004, as would be expected at this periodicity.

Therefore, even after consideration of additional archival r.v. data, the question about the multiplicity of HD 129333 remains open. The system can be either a binary with a 14–16 AU semimajor axis (but a discrepancy in the inferred mass of the secondary) or a triple with a 10 AU inner (spectroscopic) and ~25 AU outer (resolved) components. Indeed, SIMBAD does list HD 129333 as a BY Dra variable, which may indicate that the high level of chromospheric activity arises from close binarity, rather than extreme youth. However, the high photospheric Li I abundance of HD 129333 and its kinematic association with the Pleiades moving group (§ 4.2) confirm its young age. Moreover, at 10 AU semimajor axis the inferred spectroscopic companion is too distant to be synchronized with the rotation period of the primary (2.7 days; Dorren & Guinan 1994) and to thus affect its chromospheric activity. An additional close-in component would be required that should produce a short-period SB1 or SB2 spectroscopic signature, as in binary BY Dra systems. Such is not reported by DM91, however.

In deciding whether a triple system with a 24.5 yr period for the r.v. (inner) companion is a likely state for HD 129333, it is worth considering the dynamical stability of such a system. We adopt masses of 1.05, 0.5, and 0.2 $M_\odot$ for the primary, inner, and outer (resolved) companions, respectively, and apply a dynamical stability criterion from the numerical analysis of Donnison & Mikulskis (1995). Assuming prograde orbits, the Donnison & Mikulskis (1995) condition for stability as applied to HD 129333 states that the distance of closest approach of the outer companion to the barycenter of the system should be greater than 27 AU. Variations in the masses of the two companions within the determined limits do not change this requirement by more than 3–5 AU. At a projected separation of 25.0 ± 1.5 AU from the primary, the resolved companion is fully consistent with this requirement. Hence, the system can be a dynamically stable triple.

4.4. *HD 49197B: A Rare Young L Dwarf*

Our empirical knowledge of the photospheres of young (<1 Gyr) L dwarfs is currently very limited. The only confirmed such dwarfs are all companions to main-sequence stars: G196-3B (L2, 20–300 Myr; Rebolo et al. 1998), Gl 417B[5] (L4.5, 80–300 Myr; Kirkpatrick et al. 2001), the pair HD 130948B/C (L2, 300–600 Myr; Potter et al. 2002), and now HD 49197B (L4, 260–790 Myr). It is useful to expand the sample of young L dwarfs in order to study gravity-sensitive features in their spectra and to provide constraints for evolutionary models of ultracool dwarfs.

Younger L dwarfs have been reported in several open clusters: σ Ori (1–8 Myr; Zapatero Osorio et al. 1999), the Trapezium (~1 Myr; Lucas et al. 2001), and Chameleon I (1–3 Myr; López Martí et al. 2004). However, these results have not been independently confirmed. The youth of σ Ori 47 (L1.5), and hence its association with the cluster, has been recently brought into question by McGovern et al. (2004), who find that the object shows strong K I absorption at J band, characteristic of several billion year old field dwarfs. Lucas et al. (2001) determine M1–L8 spectral types for their objects in the Trapezium, using water indices defined for the $R \approx 30$ H-band spectra. They also use Burrows et al. (1997) substellar

[3] We obtained $v_{\rm rad} = -19.79 \pm 0.37$ and -21.77 ± 0.62 km s^{-1} on 2002 April 18 and 2003 February 10, respectively (L. A. Hillenbrand et al. 2004, in preparation).

[4] Maintained at the Carnegie Observatories of Washington, Pasadena, California.

[5] Gl 417B is itself considered to be resolved by Bouy et al. (2003) into two components with a 70 mas separation, equal to the diffraction limit of their *HST* WFPC2 observations.

evolutionary tracks to infer masses from *IJH* photometry. However, the deduced spectral types and the masses correlate very poorly, a result potentially traceable to the anomalous continuum shapes of their spectra (their Fig. 4), some of which appear to contain residual telluric or instrument transmission features (as seen in their Fig. 1) that the authors interpret as photospheric water absorption. Finally, in their analysis of photometrically identified brown dwarfs toward Chameleon I, López Martí et al. (2004) acknowledge that the classification of their early L dwarfs is uncertain because their locus overlaps with that of extincted M-type objects on their color-magnitude diagram (Fig. 8 in that paper).

Therefore, because of its association with a young star, HD 49197B is one of only five known young L dwarfs whose age can be determined with reasonable certainty. All five span a narrow range in spectral type: L2–L5. A program of uniform spectroscopic observations of these young L dwarf companions, undertaken in a manner similar to the NIRSPEC brown dwarf spectroscopic survey of McLean et al. (2003), promises to establish gravity-sensitive standards (as in Kleinmann & Hall 1986, for F8–M7 stars) to use in determining the ages of isolated L dwarfs.

4.5. *Substellar Companions to Main-Sequence Stars*

Until recently, only a handful of brown dwarf companions to nearby A–M stars were known from direct imaging, all at angular separations greater than $4''$ (see compilation in Reid et al. 2001). With AO technology still in its early developing stages, ground-based direct imaging observations of main-sequence stars were sensitive mostly to massive, widely separated substellar companions. From the observed dearth of brown dwarf companions to main-sequence stars at separations comparable to those in main-sequence binaries, it was inferred that the r.v. "brown dwarf desert" (for separations $\lesssim$3 AU; Campbell et al. 1988; Marcy & Benitz 1989; Marcy & Butler 2000) extended to at least 120 AU (Oppenheimer et al. 2001) or 1200 AU (McCarthy 2001; McCarthy & Zuckerman 2004), with estimates for the brown dwarf companion frequency around 1% within this separation range. From 2MASS data, however, Gizis et al. (2001) found that the brown dwarf companion fraction was much higher ($\sim$18%) at separations greater than 1000 AU from F–M0 dwarfs and consistent with that of stellar companions to G stars (DM91). Although the Gizis et al. (2001) result is based on only 3 bound companions out of 57 then known field L and T dwarfs (a fourth bound companion, GJ 1048B, has now been confirmed in the same sample by Seifahrt et al. 2004), they exclude a brown dwarf companion fraction of 1.5% at the 99.5% confidence level. Such an abrupt change in the frequency of bound brown dwarfs at 1000 AU from main-sequence stars is not predicted by any of the current brown dwarf formation scenarios. More likely would be a continuously varying substellar companion fraction from inside the r.v. brown dwarf desert at less than 3 AU out to distances greater than 1000 AU.

Recent results from more sensitive space- and ground-based surveys point to a somewhat higher frequency of substellar companions. In a survey of 45 young stars within $\sim$50 pc, the NICMOS Environments of Nearby Stars Team has reported the discovery of two confirmed brown dwarfs, TWA 5B (Webb et al. 1999; Lowrance et al. 1999) and HR 7329B (Lowrance et al. 2000), and a probable third one: the binary companion Gl 577B/C, whose components likely span the stellar/substellar boundary (Lowrance et al. 2003). A similar survey of 24 5–15 Myr old stars in the more distant ($\approx$150 pc) Scorpius-Centaurus association does not detect any plausible substellar companions (Brandner et al. 2000). Even so, the fraction of stars with substellar companions detected with NICMOS (2–3 out of 69) is markedly higher than the one reported from the two initial large-scale ground-based surveys (2 out of $\approx$390; Oppenheimer et al. 2001; McCarthy & Zuckerman 2004) and is inconsistent with the incompleteness-corrected estimate ($\leq$2%) of McCarthy & Zuckerman (2004). Furthermore, as a result of improvements in existing AO technology and the equipping of several large telescopes with newly designed high-order AO systems, recent ground-based direct imaging efforts have been more successful in detecting close-in brown dwarf companions to Sun-like primaries: Gl 86B (Els et al. 2001), HD 130948B/C (Potter et al. 2002), HR 7672B (Liu et al. 2002), and HD 49197B (this paper). All of these are at angular separations less than $3''$, as well as at projected distances less than 50 AU from their primaries, and hence inaccessible for imaging by McCarthy & Zuckerman (2004), whose survey targeted the 75–1200 AU separation range. Finally, with the natural guide star limit of AO systems being pushed to ever fainter magnitudes using curvature sensors (down to $\sim$16 mag at 0.8 μm; Siegler et al. 2003), a number of very low mass (VLM) binaries have become known, with separations as small as 1 AU. The components in these VLM binaries often straddle the stellar/substellar boundary (for a compilation see Table 4 in Close et al. 2003).

The emergent picture from these recent discoveries is that of potential deficiency of brown dwarfs at 10–1000 AU separations from main-sequence stars, although not as pronounced as in the r.v. brown dwarf desert (frequency of less than 0.5%; Marcy & Butler 2000). Based on one detection (of a binary brown dwarf companion) among 31 stars, Potter et al. (2002) set a lower limit of $3.2\% \pm 3.2\%$ for the frequency of brown dwarfs at 10–100 AU from main-sequence stars. At separations greater than 50 AU, from the NICMOS discoveries (Lowrance et al. 1999, 2000) and from their newly reported brown dwarf companion to the star GSC 08047−00232 in Horologium, Neuhäuser & Guenther (2004) report that brown dwarfs are found around $6\% \pm 4\%$ of stars. The outer scale for the Neuhäuser & Guenther (2004) estimate is not specified but is probably limited to 1000–2000 AU by the FOV of high angular resolution IR detectors (up to $40'' \times 40''$; e.g., NICMOS, or ones used behind AO) and by the distances out to which young stars are probed for substellar companions (out to 100–200 pc). By combining these estimates with the Gizis et al. (2001) estimate of $18\% \pm 14\%$ at separations greater than 1000 AU, we can conclude that, despite the small number statistics involved, there possibly exists a continuum in the frequency distribution of brown dwarf companions at separations ranging from within the r.v. brown dwarf desert ($\leq$3 AU) out to greater than 1000 AU (where brown dwarf companions are as common as stellar ones). The observed decline in the rate of occurrence of directly imaged brown dwarf companions at small separations is likely at least partially an effect of the limited sensitivity of imaging surveys to close-in low-mass brown dwarfs. New, sensitive surveys for substellar companions, such as the Palomar AO Survey of Young Stars, are poised to explore this regime in the next few years.

5. CONCLUSIONS

We have presented the observing strategy and first results from the Palomar Adaptive Optics Survey of Young Stars, aimed at detecting substellar companions to less than 400 Myr solar analogs within 160 pc of the Sun. We have discovered low-mass (0.04–0.5 $M_{\odot}$) companions to four young nearby

stars. The L4 $\pm$ 1 brown dwarf HD 49197B and the M2 $\pm$ 1 V star HD 129333B have been confirmed as companions to their corresponding primaries through follow-up astrometry and spectroscopy. Physical association in the V522 Per and RX J0329.1+0118 systems, containing, respectively, M4 $\pm$ 1 and M3 $\pm$ 2 secondaries, has been established with greater than 99.95% confidence from spectroscopy and from the expected space density of objects of similar spectral type.

The astrometry for the resolved stellar companion to HD 129333 is found to be consistent with archival r.v. data for this single-lined spectroscopic binary, indicating that the resolved and the r.v. companions may be identical. Given the inferred mass constraints on the secondary, however, the companion is then underluminous by at least 1 mag at K_S. A solution in which the star is a triple is also likely. It does not suffer from similar inconsistencies and could be dynamically stable. Because the expected mass ratio between the inner two companions of the triple is $\geq$0.46, they should be resolved as a double-lined spectroscopic binary from high-resolution infrared spectroscopy. In either case HD 129333 is confirmed to be a multiple star and hence not a true analog of the young Sun, as previously considered (e.g., Dorren & Guinan 1994; Strassmeier & Rice 1998).

The newly discovered brown dwarf HD 49197B is one of very few confirmed young (<1 Gyr) L dwarfs. It is also a member of a small number of brown dwarf companions imaged at projected separations of less than 50 AU from their host stars, i.e., at distances comparable to the giant planet zone in the solar system. The number of such companions, albeit small, has been growing steadily in recent years with the results of more sensitive imaging surveys coming online. Longer duration r.v. surveys and improvements in AO techniques are expected to further push the detection limits of each method to the point where their sensitivities overlap. Although the true extent and depth of the so-called brown dwarf desert will not be revealed until that time, increased sensitivity to substellar companions at small separation has already resulted in upward revisions of their estimated frequency.

We would like to thank Richard Dekany and Mitchell Troy for sharing with us their expertise of the Palomar AO system, Rick Burress and Jeff Hickey for assistance with PHARO, Randy Campbell, Paola Amico, and David Le Mignant for their guidance in using Keck AO, Keith Matthews and Dave Thompson for help with NIRC2, and our telescope operators Jean Mueller at the Palomar 5 m telescope and Chuck Sorenson at the Keck II telescope. We are grateful to Tom Hayward, Stephen Eikenberry, and Matthew Britton for sharing with us their ideas on AO data reduction and PSF subtraction. We thank Russel White for insightful discussions on spectroscopic binaries and for a critical review of the manuscript and the referee for detailed suggestions on chance alignment probabilities. We thank George Carlson and Donna Kirkpatrick of the Ahmanson Foundation Star Plates Archival Project for giving us access to the Mount Wilson spectroscopic survey plates. This publication makes use of data products from the Two Micron All Sky Survey, which is a joint project of the University of Massachusetts and the IPAC/California Institute of Technology, funded by NASA and the NSF. Use of the FEPS Team database has proven invaluable throughout the course of our survey. We thank John Carpenter for building and maintaining the database. Finally, the authors wish to extend special thanks to those of Hawaiian ancestry on whose sacred mountain of Mauna Kea we are privileged to be guests. Without their generous hospitality, some of the observations presented herein would not have been possible.

REFERENCES

Ali, B., Carr, J. S., Depoy, D. L., Frogel, J. A., & Sellgren, K. 1995, AJ, 110, 2415
Allende Prieto, C., & Lambert, D. L. 1999, A&A, 352, 555
Bahcall, J. N., & Soneira, R. M. 1980, ApJS, 44, 73
Baraffe, I., Chabrier, G., Allard, F., & Hauschildt, P. H. 1998, A&A, 337, 403
Baraffe, I., Chabrier, G., Barman, T. S., Allard, F., & Hauschildt, P. H. 2003, A&A, 402, 701
Bessell, M. S. 1991, AJ, 101, 662
Bessell, M. S., & Brett, J. M. 1988, PASP, 100, 1134
Bouy, H., Brandner, W., Martín, E. L., Delfosse, X., Allard, F., & Basri, G. 2003, AJ, 126, 1526
Brandner, W., et al. 2000, AJ, 120, 950
Burgasser, A. J., et al. 2002, ApJ, 564, 421
Burrows, A., et al. 1997, ApJ, 491, 856
Buscombe, W. 1998, VizieR Online Data Catalog, 3206, 0
Buscombe, W., & Foster, B. E. 1997, VizieR Online Data Catalog, 3189, 0
Campbell, B., Walker, G. A. H., & Yang, S. 1988, ApJ, 331, 902
Cardelli, J. A., Clayton, G. C., & Mathis, J. S. 1989, ApJ, 345, 245
Carpenter, J. M. 2001, AJ, 121, 2851
Carson, J., Eikenberry, S., Brandl, B., Wilson, J. C., & Hayward, T. L. 2003, in IAU Symp. 211, Brown Dwarfs, ed. E. L. Martin (Dordrecht: Kluwer), 271
Carter, B. D., Butler, R. P., Tinney, C. G., Jones, H. R. A., Marcy, G. W., McCarthy, C., Fischer, D. A., & Penny, A. J. 2003, ApJ, 593, L43
Chabrier, G., Baraffe, I., Allard, F., & Hauschildt, P. 2000, ApJ, 542, 464
Close, L. M., Siegler, N., Freed, M., & Biller, B. 2003, ApJ, 587, 407
Cox, A. N. 2000, Allen's Astrophysical Quantities (4th ed.; New York: AIP)
Cutri, R. M., et al. 2003, VizieR Online Data Catalog, 2246, 0
Dahn, C. C., et al. 2002, AJ, 124, 1170
de La Reza, R., Torres, C. A. O., Quast, G., Castilho, B. V., & Vieira, G. L. 1989, ApJ, 343, L61
Donnison, J. R., & Mikulskis, D. F. 1995, MNRAS, 272, 1
Dorren, J. D., & Guinan, E. F. 1994, ApJ, 428, 805
Duquennoy, A., & Mayor, M. 1991, A&A, 248, 485 (DM91)
Els, S. G., Sterzik, M. F., Marchis, F., Pantin, E., Endl, M., & Kürster, M. 2001, A&A, 370, L1
Frink, S., Röser, S., Neuhäuser, R., & Sterzik, M. F. 1997, A&A, 325, 613
Geballe, T. R., et al. 2002, ApJ, 564, 466
Gizis, J. E., Kirkpatrick, J. D., Burgasser, A., Reid, I. N., Monet, D. G., Liebert, J., & Wilson, J. C. 2001, ApJ, 551, L163
Gorlova, N. I., Meyer, M. R., Rieke, G. H., & Liebert, J. 2003, ApJ, 593, 1074
Green, P. J., Ali, B., & Napiwotzki, R. 2000, ApJ, 540, 992
Hale, A. 1994, AJ, 107, 306
Hartkopf, W. I., & Mason, B. D. 2003a, Sixth Catalog of Orbits of Visual Binary Stars, http://ad.usno.navy.mil/wds/orb6.html
———. 2003b, Sixth Catalog of Orbits of Visual Binary Stars: Calibration Candidates, http://ad.usno.navy.mil/wds/orb6/orb6c.html
Hartkopf, W. I., Mason, B. D., & McAlister, H. A. 1996, AJ, 111, 370
Hartkopf, W. I., Mason, B. D., & Worley, C. E. 2001, AJ, 122, 3472
Hayward, T. L., Brandl, B., Pirger, B., Blacken, C., Gull, G. E., Schoenwald, J., & Houck, J. R. 2001, PASP, 113, 105
Heintz, W. D. 1978, Geophys. Astrophys. Monogr., 15
Henry, T. J., Soderblom, D. R., Donahue, R. A., & Baliunas, S. L. 1996, AJ, 111, 439
Hillenbrand, L. A., & White, R. J. 2004, ApJ, 604, 741
Høg, E., et al. 2000, A&A, 355, L27
Kenyon, S. J., Dobrzycka, D., & Hartmann, L. 1994, AJ, 108, 1872
Kirkpatrick, J. D., Dahn, C. C., Monet, D. G., Reid, I. N., Gizis, J. E., Liebert, J., & Burgasser, A. J. 2001, AJ, 121, 3235
Kirkpatrick, J. D., et al. 2000, AJ, 120, 447
Kleinmann, S. G., & Hall, D. N. B. 1986, ApJS, 62, 501
Leggett, S. K., Allard, F., Geballe, T. R., Hauschildt, P. H., & Schweitzer, A. 2001, ApJ, 548, 908
Leggett, S. K., et al. 2002, ApJ, 564, 452
Lindegren, L. 1997, in The *Hipparcos* and Tycho Catalogues, Vol. 1, ed. M. A. C. Perryman (ESA SP-1200; Noordwijk: ESA), 87

Liu, M. C., Fischer, D. A., Graham, J. R., Lloyd, J. P., Marcy, G. W., & Butler, R. P. 2002, ApJ, 571, 519
López Martí, B., Eislöffel, J., Scholz, A., & Mundt, R. 2004, A&A, 416, 555
Lowrance, P. J. 2001, Ph.D. thesis, UCLA
Lowrance, P. J., et al. 1999, ApJ, 512, L69
———. 2000, ApJ, 541, 390
———. 2003, in IAU Symp. 211, Brown Dwarfs, ed. E. L. Martin (Dordrecht: Kluwer), 295
Lucas, P. W., Roche, P. F., Allard, F., & Hauschildt, P. H. 2001, MNRAS, 326, 695
Marcy, G. W., & Benitz, K. J. 1989, ApJ, 344, 441
Marcy, G. W., & Butler, R. P. 1998, ARA&A, 36, 57
———. 2000, PASP, 112, 137
McCarthy, C. 2001, Ph.D. thesis, UCLA
McCarthy, C., & Zuckerman, B. 2004, AJ, 127, 2871
McGovern, M. R., Kirkpatrick, J. D., McLean, I. S., Burgasser, A. J., Prato, L., & Lowrance, P. J. 2004, ApJ, 600, 1020
McLean, I. S., McGovern, M. R., Burgasser, A. J., Kirkpatrick, J. D., Prato, L., & Kim, S. S. 2003, ApJ, 596, 561
Metchev, S. A., Hillenbrand, L. A., & Meyer, M. 2002, BAAS, 34, 658
Metchev, S. A., Hillenbrand, L. A., & White, R. J. 2003, ApJ, 582, 1102
Meyer, M. R., et al. K. 2004, ApJS, 154, 422
Mohler, O. 1955, A Table of Solar Spectrum Wave Lengths, 11984A to 25578A (Ann Arbor: Univ. Michigan Press)
Montes, D., López-Santiago, J., Fernández-Figueroa, M. J., & Gálvez, M. C. 2001a, A&A, 379, 976
Montes, D., López-Santiago, J., Gálvez, M. C., Fernández-Figueroa, M. J., De Castro, E., & Cornide, M. 2001b, MNRAS, 328, 45
Morbey, C. L. 1975, PASP, 87, 689
Naef, D., Mayor, M., Beuzit, J. L., Perrier, C., Queloz, D., Sivan, J. P., & Udry, S. 2004, A&A, 414, 351
Nakajima, T., Oppenheimer, B. R., Kulkarni, S. R., Golimowski, D. A., Matthews, K., & Durrance, S. T. 1995, Nature, 378, 463
Neuhäuser, R., & Guenther, E. 2004, A&A, 420, 647
Neuhäuser, R., Sterzik, M. F., Torres, G., & Martin, E. L. 1995, A&A, 299, L13
Oppenheimer, B. R., Golimowski, D. A., Kulkarni, S. R., Matthews, K., Nakajima, T., Creech-Eakman, M., & Durrance, S. T. 2001, AJ, 121, 2189
Perryman, M. A. C., et al. 1997, A&A, 323, L49
Pinsonneault, M. H., Stauffer, J., Soderblom, D. R., King, J. R., & Hanson, R. B. 1998, ApJ, 504, 170
Potter, D., Martín, E. L., Cushing, M. C., Baudoz, P., Brandner, W., Guyon, O., & Neuhäuser, R. 2002, ApJ, 567, L133
Pourbaix, D. 2000, A&AS, 145, 215
Prato, L., Simon, M., Mazeh, T., McLean, I. S., Norman, D., & Zucker, S. 2002, ApJ, 569, 863
Press, W. H., Teukolsky, S. A., Vetterling, W. T., & Flannery, B. P. 1992, Numerical Recipes in C: The Art of Scientific Computing (2nd ed.; Cambridge: Cambridge Univ. Press)
Prosser, C. F. 1992, AJ, 103, 488
Rebolo, R., Zapatero Osorio, M. R., Madruga, S., Bejar, V. J. S., Arribas, S., & Licandro, J. 1998, Science, 282, 1309
Reid, I. N., Gizis, J. E., Kirkpatrick, J. D., & Koerner, D. W. 2001, AJ, 121, 489
Reid, I. N., et al. 2003, AJ, 125, 354
Rucinski, S. M., & Krautter, J. 1983, A&A, 121, 217
Scardia, M. 1979, Astron. Nachr., 300, 307
Seifahrt, A., Neuhäuser, R., & Mugrauer, M. 2004, A&A, 421, 255
Siegler, N., Close, L. M., & Freed, M. E. 2003, Proc. SPIE, 4839, 114
Slesnick, C., Hillenbrand, L. A., & Carpenter, J. M. 2004, ApJ, 610, 1045
Soderblom, D. R. 1985, AJ, 90, 2103
Soderblom, D. R., & Clements, S. D. 1987, AJ, 93, 920
Soderblom, D. R., Stauffer, J. R., MacGregor, K. B., & Jones, B. F. 1993, ApJ, 409, 624
Söderhjelm, S. 1999, A&A, 341, 121
Stauffer, J. R., Schultz, G., & Kirkpatrick, J. D. 1998, ApJ, 499, L199
Stauffer, J. R., et al. 1999, ApJ, 527, 219
Sterzik, M. F., Durisen, R. H., Brandner, W., Jurcevic, J., & Honeycutt, R. K. 1997, AJ, 114, 1555
Strassmeier, K. G., & Rice, J. B. 1998, A&A, 330, 685
Thompson, D., Egami, E., & Sawicki, M. 2001, The Keck Near-Infrared AO Camera: Pre-Ship Testing, http://www2.keck.hawaii.edu/inst/nirc2/preship_testing.pdf
Troy, M., et al. 2000, Proc. SPIE, 4007, 31
van Dokkum, P. G. 2001, PASP, 113, 1420
van Leeuwen, F. 1999, A&A, 341, L71
Ventura, P., Zeppieri, A., Mazzitelli, I., & D'Antona, F. 1998, A&A, 334, 953
Wallace, L., & Hinkle, K. 1997, ApJS, 111, 445
Wallace, L., Meyer, M. R., Hinkle, K., & Edwards, S. 2000, ApJ, 535, 325
Webb, R. A., Zuckerman, B., Platais, I., Patience, J., White, R. J., Schwartz, M. J., & McCarthy, C. 1999, ApJ, 512, L63
Wilson, R. E., & Joy, A. H. 1950, ApJ, 111, 221
Wizinowich, P., et al. 2000, PASP, 112, 315
Wright, J. T., Marcy, G. W., Butler, R. P., & Vogt, S. S. 2004, ApJS, 152, 261
Zapatero Osorio, M. R., Béjar, V. J. S., Rebolo, R., Martín, E. L., & Basri, G. 1999, ApJ, 524, L115
Zuckerman, B., & Becklin, E. E. 1992, ApJ, 386, 260
Zuckerman, B., Song, I., Bessell, M. S., & Webb, R. A. 2001a, ApJ, 562, L87
Zuckerman, B., Song, I., & Webb, R. A. 2001b, ApJ, 559, 388
Zuckerman, B., & Webb, R. A. 2000, ApJ, 535, 959